Citation: Pueyo, E.L., Rodríguez-Pintó, A., Serra-Kiel, J., Barnolas, A., 2022. The chronology and rotational kinematics in the South-Eastern Jaca Basin (Southern Pyrenees): Las Bellostas section. Geologica Acta, 20.12, 1-29.
DOI: 10.1344/GeologicaActa2022.20.12

The chronology and rotational kinematics in the South-Eastern Jaca Basin (Southern Pyrenees): Las Bellostas section

Emilio L. Pueyo[1,2] Adriana Rodríguez-Pintó[3] Josep Serra-Kiel[4] Antonio Barnolas[5]

[1]Instituto Geológico y Minero de España (IGME) CSIC, Unidad de Zaragoza
C/M. Lasala 44, 9ºB, 50006, Zaragoza, Spain. E-mail: unaim@igme.es

[2]Associated Unit in Earth Sciences IGME (CSIC)/Universidad de Zaragoza
Spain

[3]Freelance Geologist
E-mail: adrianaropi14@gmail.com

[4]Museu de Ciències Naturals de Barcelona, Departament de Paleontologia
Passeig Picasso s/n, 08003 Barcelona, Spain

[5]Instituto Geológico y Minero de España (IGME) CSIC
Ríos Rosas, 23, 28003, Madrid, Spain toni.barnolas@gmail.com

ABSTRACT

Despite the large number of magnetostratigraphic studies in the South Pyrenean Basin aiming to calibrate the basin chronostratigraphy and the biostratigraphic scales, the South Eastern Jaca Basin remains unexplored from this perspective, and its relation with the Ainsa Basin is not fully understood. In this work we contribute with new magnetostratigraphic data from the 950m thick Las Bellostas section, located in the northern hinge of the Balzes anticline. Well-proven primary signal (positive fold test and two pseudo-antiparallel polarities) supported by numerous primary data in the surroundings allow us building a reliable local polarity sequence of eight magnetozones (from R1 to N4). Additionally, seven new biostratigraphic samples (*Nummulites* and *Assilina*) in the lower part of the section (marine environment) allows tightening the section to the Geomagnetic Polarity Time Scale (GPTS) and proposing a refined age model for the southeastern Jaca Basin. The section starts in the Boltaña Fm., of Cuisian age (Shallow Benthic Zone, SBZ11), is followed by a sedimentary gap from C22n to C20n as witnessed by biostratigraphic data (SBZ11 underneath the hiatus and SBZ16 just atop). The deltaic Sobrarbe Fm can be tracked until the C19n (Late Lutetian). From this point (200m) until the top of the section (950m), at least, the entire C18n chron can be recognized within the molassic Campodarbe Fm (C18n.2n-C18n.1r and C18n.1n) (Bartonian) equivalent to the West to the prodeltaic Arguis marls Fm. The Middle Cusian (SBZ11) to Middle Lutetian (SBZ15) stratigraphic hiatus is, in part, enhanced by the structural position at the hinge of the Balzes anticline. These new chronostratigraphic constraints help refining the W-E and N-S stratigraphic relationships in the eastern Jaca Basin and in the Ainsa Basin. This section also allows us to accurately refine the kinematics of the rotational activity in the eastern External Sierras. The significant difference in magnetic declination along the section and neighboring paleomagnetic data from the Balzes anticline (from ≈70º clockwise at the base of the stratigraphic section to non-significant at the top) together with the new age model for the Eastern Jaca Basin help characterizing the rotational activity of the Balzes thrust sheet. The rotation took place between chrons C20r (Middle Lutetian; 45Ma) and C17 (Lower Priabonian 37-38Ma) in agreement to nearby structures (Boltaña, Pico del Aguila anticlines) but clearly diachronic to western ones (Santo Domingo anticline). Besides, the rotational

activity seems to follow a linear and continuous pattern (velocity 9-11º/Ma, R: 0.83-0.96) in contrast to closer structures that show two distinct rotational velocities (*i.e.* Boltaña). These new data still let open the debate on the rotational kinematics along the South Pyrenean basal thrust.

KEYWORDS | **Magnetostratigraphy. Rotational kinematics. Pyrenean frontal thrust. Ypresian. Cuisian. Lutetian. Bartonian.**

INTRODUCTION

Unravelling the 4D evolution of fold-and-thrust-belts and deformed sedimentary basins have been classically tackled by means of the study of syntectonic sediments (Riba, 1976) which allows constraining the timing of the involved geological processes. In the past, the chronological framework was only based on biostratigraphical data but since the development of the first Geomagnetic Polarity Time Scales in the 60's (Cox *et al.*, 1963), magnetostratigraphic studies have helped yielding a more robust, continuous, accurate and reliable chronological framework, especially in syntectonic basins (Burbank and Raynolds, 1988; Heller and Paola, 1992). Magnetostratigraphy has some advantages over other chronological approaches (*e.g.* fission tracks) and allows for an efficient, semi-continuous and independent chronostratigraphic frame to be achieved, especially when very long stratigraphic series (>1000m) are studied. This is because it is based on an absolute external property of the Earth (changes in magnetic polarity) that imprints a distinct pattern of recorded magnetic chrones and, in cases of long sections, several isochrons can be obtained. Further tightening with biostratigraphic scales in the GPTS allows achieving a very robust chronostratigraphic frame. However, the limitations of magnetostratigraphy must be taken into account and several studies have helped improving the resolution, estimating the uncertainty and the drawbacks of the technique (Deenen *et al.*, 2011; Johnson and McGee, 1983; Opdyke and Channell, 1996; Talling and Burbank, 1993; Tauxe and Gallet, 1991; Vandamme, 1994).

Dealing with deformational processes in fold and thrust belts, the characterization of rotational movements has also been led by paleomagnetism since more than six decades (Norris and Black, 1961) because the magnetic remanence is the only rock property that can be unambiguously referred to and external and usually well-known reference system in the undeformed stage (see recent reviews by Pueyo *et al.*, 2016; Sussman and Weil, 2004 and references therein). Syntectonic sediments are key- stones to decipher other kinematic variables (folding, thrusting, etc.) as well as their paces in fold and thrust belts especially when combined with magnetostratigraphic sections (among others Burbank *et al.*, 1992; Chen *et al.*, 2002). However, and beyond the characterization of Vertical-Axis-Rotations (VAR), many questions remain unsolved to fully understand the architecture and rotational kinematics of deformational systems, particularly at the fold and thrust belt scale (Oliva-Urcia and Pueyo, 2019). Among them, many efforts must be done to attain a precise timing of the rotation process as well as the determination of the rotation velocities and their implications in the overall kinematics.

Due to the high degree of preservation, the outcropping of abundant syntectonic series and the exceptional chronostratigraphic framework based on numerous and outstanding biostratigraphic (Serra-Kiel *et al.*, 1998, 2003, 2020 and references therein) and magnetostratigraphic studies (see recent reviews by Garcés *et al.*, 2020; Pérez-Rivarés *et al.*, 2018; Vinyoles *et al.*, 2020) together with the occurrence of VAR (witnessed by plentiful paleomagnetic studies; Pueyo *et al.*, 2017), the Southern Pyrenees is an exceptional location to characterize the rotational kinematics of thrust fronts. Pioneer works at the Pico del Águila anticline (Pyrenean sole thrust) in the Central External Sierras (Pueyo *et al.*,2002) were followed by others in closer structures; the Boltaña anticline (Mochales *et al.*, 2012a) and the Aínsa Basin (Muñoz *et al.*, 2013), pilot studies in the Mediano anticline (Beamud *et al.*, 2017) to the East and in the Santo Domingo anticline to the West (Pueyo *et al.*, 2021). The rotation velocity of the Balzes anticline was also preliminarily studied in its northern part (Rodríguez-Pintó, 2013 and Rodríguez- Pintó *et al.*, 2016). A set of nine standard paleomagnetic sites where discretely located along the Isuela 800m thick section nearby Las Bellostas village (from the Eocene marine rocks to the base of the Campodarbe Fm.). However, the large spacing among sites and the limited quality of the signal in part of the dataset precluded an accurate timing of the rotational activity and the kinematics of this structure.

The new magnetostratigraphic section introduced in this paper (Las Bellostas section) allows a much better and reliable characterization of the rotational kinematics of this fold and the underneath structures and helps refining the chronostratigraphic frame in the easternmost sector of the the Jaca Basin as well as the chronostratigraphic relationships with nearby rock formations.

GEOLOGICAL SETTING

The South-Central Pyrenees

The Pyrenees were built during Late Cretaceous to Miocene times as a consequence of the convergence and

the subsequent collision of the African and Euroasiatic plates (Muñoz, 1992; Pocoví, 2019). In the southwestern Pyrenees, the main cover thrust-sheets are the Internal Sierras, the Jaca Basin and the External Sierras (Casas and Pardo, 2004; Labaume *et al.*, 2016; Labaume and Teixell, 2018; Meresse, 2010; Millán *et al.*, 2006; Muñoz, 2019; Oliva-Urcia, 2018; Toro *et al.*, 2021). This study is located in the southeastern part of the Jaca molassic basin and in the northern sector of the External Sierras (Fig. 1). In that sector, the South Pyrenean sole thrust displays a large-scale footwall ramp. The External Sierras front, to theSouth, displays complex geometric relationships among several imbricate thrust sheets (Anastasio and Holl, 2001; McElroy, 1990; Millán, 1996; Santolaria *et al.*, 2020). The study area is located at the northern part of the Balzes-Boltaña thrust sheet (Millán, 1996) and there, the outcropping Eocene marine platform sediments show structural and stratigraphic continuity with the very thick overlying Campodarbe Fm.

Syntectonic deposits allow distinguishing two main deformation events in this region (Millán *et al.*, 2000 and references herein). The first one is very diachronic along-strike but Lutetian in age in the study area, it is usually related to the activity of the Gavarnie basement nappe, and witnessed by the outstanding growth strata in the western limb of the Balzes anticline (Barnolas and Gil-Peña, 2001; Rodríguez-Pintó *et al.*, 2016). The second one (Oligocene-Miocene) is widely recognized in other portions of the External Sierras in relation to the emplacement to the younger Guarga basement thrust sheet that produces the large scale thrust ramp and involves the Campodarbe and Uncastillo formations (Anastasio *et al.*, 2020; Arenas *et al.*, 2001; Luzón, 2005; Millán, 1996; Oliva-Urcia *et al.*, 2016, 2019).

Chronological framework

The southern Pyrenean basin has been the target of numerous magnetostratigraphic studies and displays a well-constrained chronostratigraphic framework (Barnolas *et al.*, 2019) (Fig. 2). The stratigraphic units along the eastern limb of the Boltaña anticline were first dated by Bentham and Burbank (1996) and then fully reviewed by Mochales *et al.* (2012b) except for the upper continental part that was recently revisited (Vinyoles *et al.*, 2020). Therefore, a complete and reliable magnetostratigraphic dating is available from the Ypresian *Alveolina*-limestones (C24r) to the upper Escanilla sandstone Fm. (C17n) Bartonian in age. It is worth clarifying at this point, that the Ypresian stage has been classically divided into Ilerdian (see recent review by Pujalte *et al.*, 2009) and Cuisian (Schaub, 1992) in the Pyrenees.

To the west, the pioneer work by Hogan and Burbank (1996) from the top of the Guara Fm. to the top of the molassic Campodarbe and Bernués fms. were later on totally reviewed along the Cusian-Lutetian boundary (Gabardiella section; Rodríguez-Pintó *et al.*, 2017), the Lutetian carbonate platform Guara Fm. (Isuela section by Rodríguez-Pintó *et al.*, 2012a, 2019 and other western sections by Silva-Casal *et al.*, 2019, see overview in Silva-Casal *et al.*, 2021), the Bartonian prodeltaic marls of the Arguis Fm. (Kodama *et al.*, 2010) and the transitional deposits of the Belsué Fm. (Garcés *et al.*, 2014; Valero *et al.*, 2020). Additionally, the marine platform deposits in the southern sector of the Balzes anticline are also dated in the San Pelegrin section (Rodríguez-Pintó *et al.*, 2013a). To the North, the Yebra de Basa section (Hogan, 1993; Hogan and Burbank, 1996) was revisited in the Lutetian-Bartonian portion by Oms *et al.* (2003) and also by Vinyoles (2021) in the Bartonian-Priabonian part.

Recently, some efforts have been done to establish stratigraphic correlations based on the vast dataset of magnetostratigraphic sections available in the Pyrenees (Garcés *et al.*, 2020; Vinyoles *et al.*, 2020). Although, in the eastern portion of the Jaca Basin the absence of previous magnetostratigraphic studies has precluded establishing accurate correlations, this exceptional dataset and chronostratigraphic framework is very helpful to constrain our results.

MATERIAL AND METHODS

Biostratigraphy

We sampled seven different stratigraphic beds located in the lower marine part of Las Bellostas section. The lowermost sample corresponds to the Boltaña Fm., while the others were collected in the Sobrarbe Fm. (Fig. 3). The larger foraminifera studied in this section (*Nummulites* and *Assilina*) were obtained as isolated specimens. The original samples were disaggregated in water, oxygen peroxide and Na_2CO_3 solution and later sieved with sieves with mesh apertures of 1.0, 0.5 and 0.2mm. Individual specimens were separated, splitted along its equatorial sections and finally polished in order to observe the internal characters needed for their taxonomical determination. The studied material is housed at the Museu de Ciències Naturals de Barcelona with the following register numbers: MGB 90398 (site BA01), MGB 90399 (site BA02), MGB 90400 (site BA03), MGB 90401 (site BA04), MGB 90402 (site BA05), MGB 90403 (site BA06) and MGB 90404 (site BA07).

Magnetostratigraphy

Sampling

A new magnetostratigraphic section, 950m in thickness, with 124 levels spaced about 4-7m, was sampled. Sampling

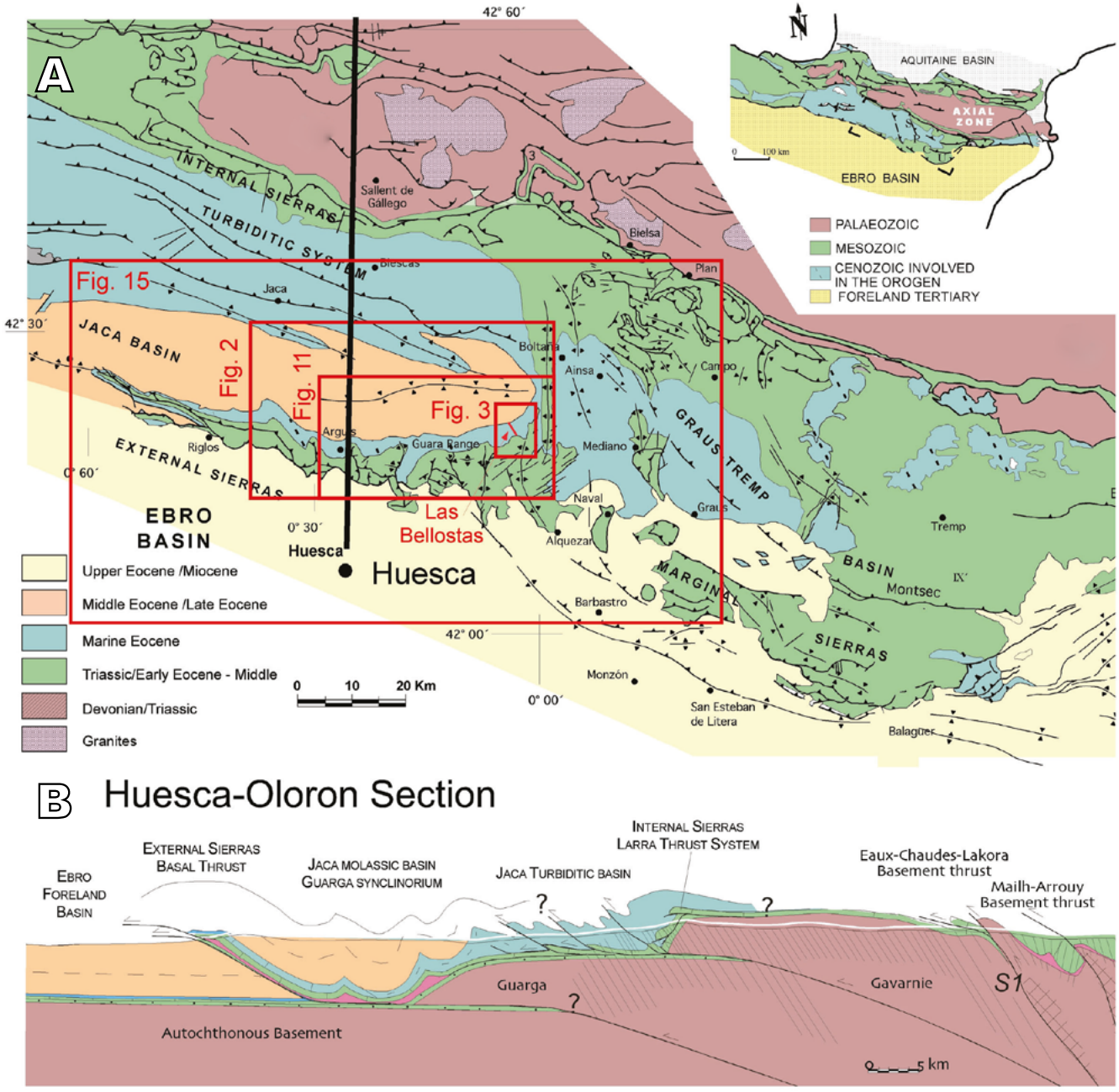

FIGURE 1. Location of study area in the South Western Central Pyrenees. A) Geological map modified from Millán (1996) and Pueyo *et al.* (1997). B) Huesca-Oloron section by Casas and Pardo (2004).

combined drilled cores at the base of the section (most samples) and oriented blocks in the remaining part of the section. Cores were drilled with a water-cooled, gas-powered machine and all samples were oriented in-situ using a magnetic compass. Oriented blocks were cut in regular cubes (2cm side). The new section improves the limited continuity of previous sampling based on only nine discrete standard paleomagnetic (RI-) sites (Rodríguez-Pintó *et al.*, 2016). The section (Fig. 3) starts in the northern part of the Upper Balzes canyon (south of Las Bellostas village) in the Cuisian marine limestones where the lowermost sample BA07 is located, then it crosses the Cuisian/Lutetian unconformity, the overlying Upper Guara (5m), and continues along the Sobrarbe deltaic Fm. (where the remaining biostratigraphic samples are located). A paraconformity with the Campodarbe fluvial Fm. is found at 185m and the sampled continental section continues more than 765m above this boundary.

FIGURE 2. Magnetostratigraphic framework. Orthophoto of the eastern Jaca basin, western Ainsa basin and the External Sierras showing the location of magnetostratigraphic sections available from the region (including Las Bellostas, see mode details in Fig. 3). The position of the stratigraphic correlation panel (Fig. 13) is also displayed.

Laboratory procedures

The initial measuring of the magnetic susceptibility was done at the University of Zaragoza (Geotransfer group) using a KLY-4 (AGICO). The paleomagnetic measurements were carried out at the Paleomagnetic laboratory of the University of Burgos (Spain). In total, 124 standard specimens were thermally demagnetized. Detailed stepwise thermal (TH) demagnetizations were performed up to 675ºC (13 steps of demagnetization, increments between 25-60ºC) with a TD-48 SC (ASC Scientific) and a MMTD80 (Magnetic Measurements) furnaces. The main demagnetization sequence was: 20, 180, 240, 290, 340, 380, 430, 480, 520, 570, 620, 650, 675ºC for most of samples. Magnetization measurements were taken with a 2G superconducting cryogenic magnetometer (model 755-1.65). The system is magnetically armored with a self-balanced set of Helmholtz coils (6m^3) coupled with a triaxial MR-3 fluxgate magnetometer (Stefan Mayer Inst.) Isothermal Remanent Magnetization (IRM) acquisition curves, and thermal demagnetization of three components IRM (Lowrie's test, 1990), were accomplished to characterize the rock magnetism in a small set of sister samples using M2T-1 pulse magnetizer (Ferronato). Progressive IRM acquisition (fourteen steps) was performed with increments of 25mT up to 100mT, then 50mT up to 200, 100mT up to 400mT, 200mT up to 800mT and three additional steps at 1.2, 1.6 and 2T. For the Lowrie's test, a 2T field was applied along the z-axis (hard coercivity phase), an intermediate one of 0.4T along the y-axis (medium) and a 0.12T field along the x-axis (soft). The thermal demagnetization routine was similar to the one applied to demagnetize the Natural Remanent Magnetization (NRM). Magnetic susceptibility measurements were carried out with KLY-4 Kappabridge software (Geofyzika Brno) during the thermal treatment to control for possible mineralogical changes. Additional acquisition of IRM analyses on a wider set of samples, were also carried out at the CACTI Magnetometry laboratory (Institute of technology and scientific support for research from the University of Vigo), using a 2G Enterprises superconducting magnetometer (model SRM- 755).

RESULTS

Lithostratigraphy of the Las Bellostas section

The studied Las Bellostas section is located in the transitional zone between the External Sierras and the Guarga syncline, over the Balzes anticline hinge. This

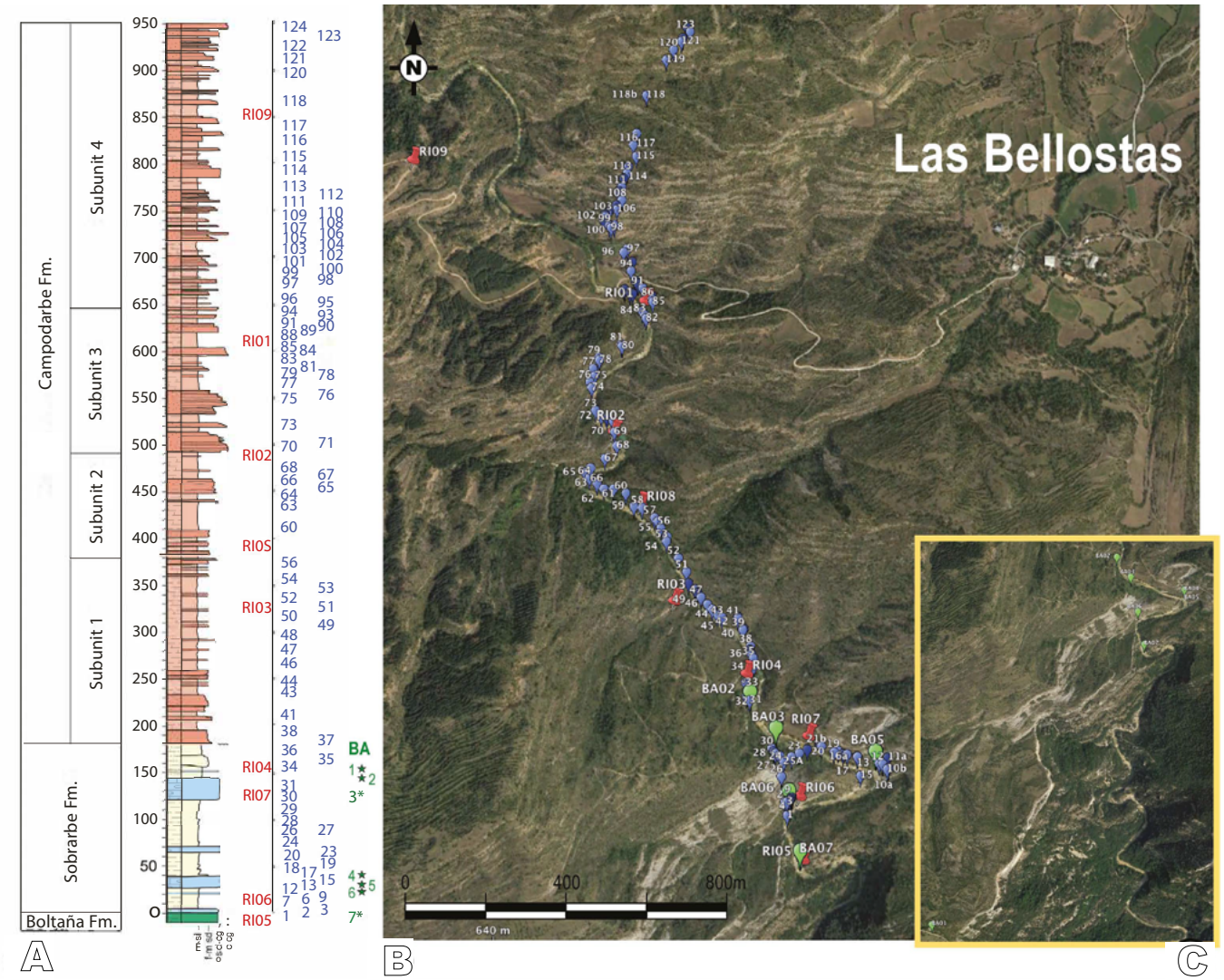

FIGURE 3. A) Las Bellostas stratigraphic section and B) orthophoto with location of samples. Blue dots: magnetostratigraphic samples. Red pins: previous standard paleomagnetic (Ri-x) sites. BA0-X green points: biostratigraphic samples. C) Biostratigraphic data alone.

anticline, detached on the Triassic saline units (Millán, 1996), includes a thick Ypresian carbonate (*Alveolina*-limestone Fm.) and the mixed carbonate-siliciclastic succession of the Boltaña Fm. (Barnolas *et al.*, 2019; Barnolas and Gil-Peña, 2001; Rodríguez-Pintó *et al.*, 2013a) cropping out in the Balzes canyon. The Balzes anticline grew up synchronously with the lower-middle Lutetian (SBZ13 to SBZ15 p.p.) carbonate sedimentation (Lower and Middle Guara in the sense of Rodríguez-Pintó *et al.*, 2012a), as inferred by growth strata exposed in its western anticline limb (Barnolas and Gil-Peña, 2001; Rodríguez-Pintó *et al.*, 2016). The upper part of the Guara Fm. (Upper Guara in the sense of Rodríguez-Pintó *et al.*, 2012a; upper middle to late Lutetian in age; SBZ 15 pp. to SBZ 16), which rests in stratigraphic continuity with the entire Guara Fm at the hinge of the Rodellar syncline (Mascún canyon), to the West of the Balzes anticline (see Fig. 2), becomes progressively unconformable over previous Lower and Middle Guara limestones to the East, in the Balzes anticline western limb. This situation defines an angular unconformity that reaches the Boltaña Fm. (middle Cuisian) in the hinge zone of Balzes anticline (Barnolas and Gil-Peña, 2001). The Upper Guara shallow marine carbonate facies of the Mascún- Santa Marina outcrops (Barnolas and Gil-Peña, 2001; Rodríguez-Pintó *et al.*, 2012b, 2016), interfingers eastwards with the deltaic facies of the Sobrarbe Fm., as exposed between the Santa Marina section (Rodríguez-Pintó *et al.*, 2012b) and the Las Bellostas section. In Las Bellostas section the Sobrarbe Fm. shows the typical deltaic facies-associations except for its basal transgressive level, which continues displaying the shallow-marine limestone facies that are more characteristic of the Upper Guara Mb.

The Campodarbe Fm. deposits (Soler and Puigdefàbregas, 1970, redefined by Puigdefàbregas, 1975) overlay the Sobrarbe Fm. The contact between both formations corresponds to a regional unconformity, and the characteristic transitional facies developed on top of the Sobrarbe delta in the Ainsa Basin, are absent in Las Bellostas section. In the original definition of the Campodarbe Fm., *i.e.* continental red beds below the Oligocene conglomerates (Soler and Puigdefàbregas, 1970; Puidefàbregas, 1975), this unit is laterally equivalent to the marine prodeltaic and deltaic sequences of the Arguis marls and the Belsúe-Atarés sandstones and limestones, Bartonian and early Priabonian in age (Canudo *et al.*, 1988; Costa *et al.*, 2010; Kodama *et al.*, 2010; Puigdefàbregas, 1975). Furthermore, according to Puigdefàbregas (1975) the Campodarbe Fm. is limited at top by the Torruéllola conglomerate. The studied interval in the Campodarbe Fm. corresponds to the Bibán facies as defined in Puigdefàbregas (1975) and to the unit 20 of Montes-Santiago (2009).

In this context, the studied section (Fig. 3) starts in the sandstones and sandy limestones of the Boltaña Fm., underlying the unconformable Upper Guara Mb basal limestones. The transgressive Upper Guara limestone consists of packstones-grainstones, rich in miliolids and larger foraminifera (alveolinids and nummulitids) that indicate inner shallow platform facies. This limestone level bed shows a slightly deepening upward sequence, evidenced by a shift in the micropaleontological content, ranging from miliolids to *Alveolina*. Its transition to the overlying Sobrarbe Fm is sharp and represents a flooding (drowning) surface. The Sobrarbe Fm consists of slightly bioturbated marls and silty marls in their lower part, which grade upwards to a siltier and sandier sequence. In its upper part, some thickening upward sequences are topped by cross-bedded sandstone channels (Fig. 3). This type of sequences reflects the general regressive trend of the Sobrarbe Fm. observed in the Ainsa Basin (Dreyer *et al.*, 1999; De Federico, 1981) and results in the stacking of successive individual regressive siliciclastic sequences separated by transgressive ones. The transgressive sequences are built up by thick nummulitic-rich levels topped, occasionally, by small coral patch reefs (Dreyer *et al.*, 1999; De Federico, 1981; Mateu-Vicens *et al.*, 2012). In Las Bellostas section (Fig. 3), five such nummulitic levels are recognized, mainly containing A and B forms of *N. perforatus* phyllum species in the sense of Schaub (1981) (see biostratigraphy section for details).

In the studied succession, the Campodarbe Fm. (Fig. 3) consists of an alternation of channelized sheet sandstones and conglomerates with inter-fluvial mudstone intervals, including siltstones and fine- grained sandstones, interpreted as overbank deposits. Changes in the sedimentary characteristics of the channelized and inter-fluvial facies along the succession allow defining four subunits. The first one, between meters 180 to 375 of the log (Fig. 3), consists of sheet-type commonly multi-storey fluvial channels with a thinning-upward sequence. They are filled in by cross-bedded sandstones and microconglomerates with clasts of Variscan origin. These channel sequences usually end with rippled and bioturbated fine-grained sandstones and siltstones. The mudstone inter-fluvial intervals include bioturbated light-red clays and a variable amount of rippled and bioturbated fine-grained tabular sandstones and siltstones facies.

Subunit 2, between meters 375 to 490 of the log (Fig. 3), includes similar multi-storey sheet-type fluvial channels filled by medium to coarse-grained sandstones and conglomerates. The Variscan clasts coexist here with a small amount of clasts coming from Mesozoic and Cenozoic source rocks. This subunit shows a significant change in the mudstone inter-fluvial interval, displaying dominant dark red facies with verticalized bioturbations in the lower part of this section.

Subunit 3, between meters 490 to 645 of the log (Fig. 3), includes two >15m thick, conglomeratic and coarse sandstone, multi-storey sheet-type channels in their lower part, separated by thin inter-fluvial mudstone deposits. Its upper part is dominated by thick intervals of inter-fluvial light red mudstone deposits, including intercalations of sheeted and bioturbated fine-grained sandstones and siltstones (overbank deposits), which alternate with up to 10m thick, sheet multi-storey channels of conglomeratic and coarse-grained sandstones. In this section, the occurrence of Mesozoic and Cenozoic pebbles in the conglomeratic multi-storey channels increases to reach up to 60%. However, some channels still show predominant clasts of Variscan source.

Subunit 4, from meter 645 to the top of the studied succession (Fig. 3), shows a similar pattern of alternation of sheet-type channels and inter-fluvial light red bioturbated mudstones including fine-grained bioturbated sandstones and siltstones (overbank deposits). The conglomerate clasts display a similar proportion of Variscan and Mesozoic-Cenozoic pebbles as in the underlying subunit. The main difference of this section is that the multi-storey channels usually end with meandering cannel deposits attested by the presence of point-bar geometries. Also, in the interval between samples and, conglomeratic channels contain abundant giant oncolites, frequently developed around phytoclasts.

Biostratigraphy of the Las Bellostas section

Results of the biostratigraphic study were summarized in Table 1. In Las Bellostas section, the simple BA07 contains

Assilina laxispira DE LA HARPE, 1926 (Fig. 4A, B, C) and *Nummulites rotularius* DESHAYES, 1838 (Fig. 4D, E, F) indicating a Middle Cuisian age, or Shallow Benthic Zone (SBZ) SBZ11 according to Schaub (1981) and Serra-Kiel *et al.* (1998). The samples BA06, BA05 and BA04 contain *Nummulites tavertetensis* REGUANT ET CLAVELL, 1967 (Fig. 4I, J, K) and *Nummulites crassus* BOUBÉE, 1831 (Fig. 4L, N, M, O, P) indicating a late Middle Lutetian age or SBZ15 (Serra-Kiel *et al.*, 1998). The samples BA03, BA02 and BA01 contain *Nummulites deshayesi* D'ARCHIAC ET HAIME, 1853 (Fig. 4Q to Y) and *Nummulites beaumonti* D'ARCHIAC ET HAIME, 1853 (Fig. 4G,H) indicating a Late Lutetian age or SBZ16 (Serra-Kiel *et al.*, 1998).

Magnetostratigraphy of the Las Bellostas section

Rock magnetism

NRM in Las Bellostas section ranges from 114 10^{-6}A/m to 1619 10^{-6}A/m, and a mean value of 507 10^{-6}mA/m. With an average of 91 10^{-6} S.I. units, a weak paramagnetic behavior can be inferred from bulk susceptibility in the sample set. Minimum and maximum values range from 38 to 430 10^{-6} S.I. units respectively.

Stepwise IRM acquisition and 3-axes IRM demagnetization at peak fields of 0.12, 0.4 and 2 Tesla (Lowrie's, 1990 test); depict the occurrence of low, medium and high coercivity phases in different proportions but depending upon the lithology (Fig. 5). According to IRM acquisition diagrams, infan–delta lithologies (blue marls and marly siltstones of the Sobrarbe Fm.), curves are almost saturated at the lowest field, and not completely saturated in most of the red siltstones (Campodarbe Fm.), showing the presence of medium/high coercitivity magnetic minerals.

Three axes IRM thermal demagnetization diagrams (Fig. 5) also show the occurrence of magnetite; drop of the low (0.12T) coercivity component at 580ºC. Some undifferentiated iron sulphides can be recognized by a drop of the 0.4T coercivity component between 200-400ºC. Finally, high and medium coercivity minerals such as goethite and hematite are present in sandstones and siltstones of the continental Campodarbe Fm. (0.4 and 2T components falling at very low and very high temperaturas respectively). All in all, rock magnetism is coherent with those data described in earlier works in the Jaca Basin and External Sierras in the same rock formations (Larrasoaña *et al.*, 2003; Pueyo-Anchuela *et al.*, 2012; Rodríguez-Pintó, *et al.*, 2016; Oliva-Urcia *et al.*, 2019).

Paleomagnetic directions

NRM demagnetization vectors were plotted in Zijderveld diagrams (1967). Individual directions were calculated by endpoint and Principal Component Analyses (PCA, Kirschvink, 1980) using the VPD software Ramón *et al.* (2017). Fisher (1953) statistics were applied to calculate individual site means as well as running averages along the profile. Stereographic projections were done using the Stereonet software (Allmendinger *et al.*, 2013).

TABLE 1. Biostratigraphic data of the Las Bellostas section including SBZ biozone assignation after Serra-Kiel *et al.* (1998) as well as the register codes of the Museu de Ciències Naturals de Barcelona

MGB	SAMPLES	TAXON	SBZ	AGE
MGB 90398	BA 01	Nummulites deshayesi D'ARCHIAC & HAIME, 1853,	SBZ 16	Upper Lutetian
MGB 90399	BA 02	Nummulites deshayesi D'ARCHIAC & HAIME, 1853, Nummulites beaumonti D'ARCHIAC & HAIME, 1853,	SBZ 16	Upper Lutetian
MGB 90400	BA 03	Nummulites deshayesi D'ARCHIAC & HAIME, 1853,	SBZ 16	Upper Lutetian
MGB 90401	BA04	Nummulites tavertetensis REGUANT & CLAVELL, 1967,	SBZ 15	Upper/Middle Lutetian
MGB 90402	BA 05	Nummulites tavertetensis REGUANT & CLAVELL, 1967,	SBZ 15	Upper/Middle Lutetian
MGB 90403	BA 06	Nummulites crassus BOUBEE, 1831,	SBZ 15	Upper/Middle Lutetian
MGB 90404	BA 07	Assilina laxispira DE LA HARPE, 1926, Nummulites rotularius DESHAYES, 1838	SBZ 11	Middle Cuisian

Zijderveld diagrams reveal (Figs. 5; 6) a low temperature viscous component up to 180º-240ºC, similar to the present geomagnetic field. At higher temperatures (240º to 675ºC), they display normal and reverse polarity components decaying towards the origin in most cases. In average, the Characteristic Remanent Magnetization (ChRM) can be defined by 6 demagnetization steps within this interval. From a lithological point of view, individual directions are calculated between 240º–580ºC steps, for grey mudstones and limestones facies (Sobrarbe and Guara fms.), and up to 675ºC in a significant set of detrital continental facies (Campodarbe Fm.). The high temperature component is assumed to be the ChRM of this dataset.

Occurrence of poor quality data (low intensities, poor definition, neoformation of magnetic phases upon heating in laboratory), lead us to classify ChRM directions into three quality types (Q-). Type 1 vectors (36%) displayed a Maximum Angular Deviation (MAD)<15º, and were fitted by ≥4 demagnetization steps, ChRM's are addressed clearly to the origin. Type 2 vectors (34%) with MAD≥15º, but clear directions not always addressed to the origin but with an unambiguous polarity. Type 3 vectors (20%), with MAD≥15°, but weaker and/or noisier directions. The remaining dataset (10%) was not considered because of unstable directions.

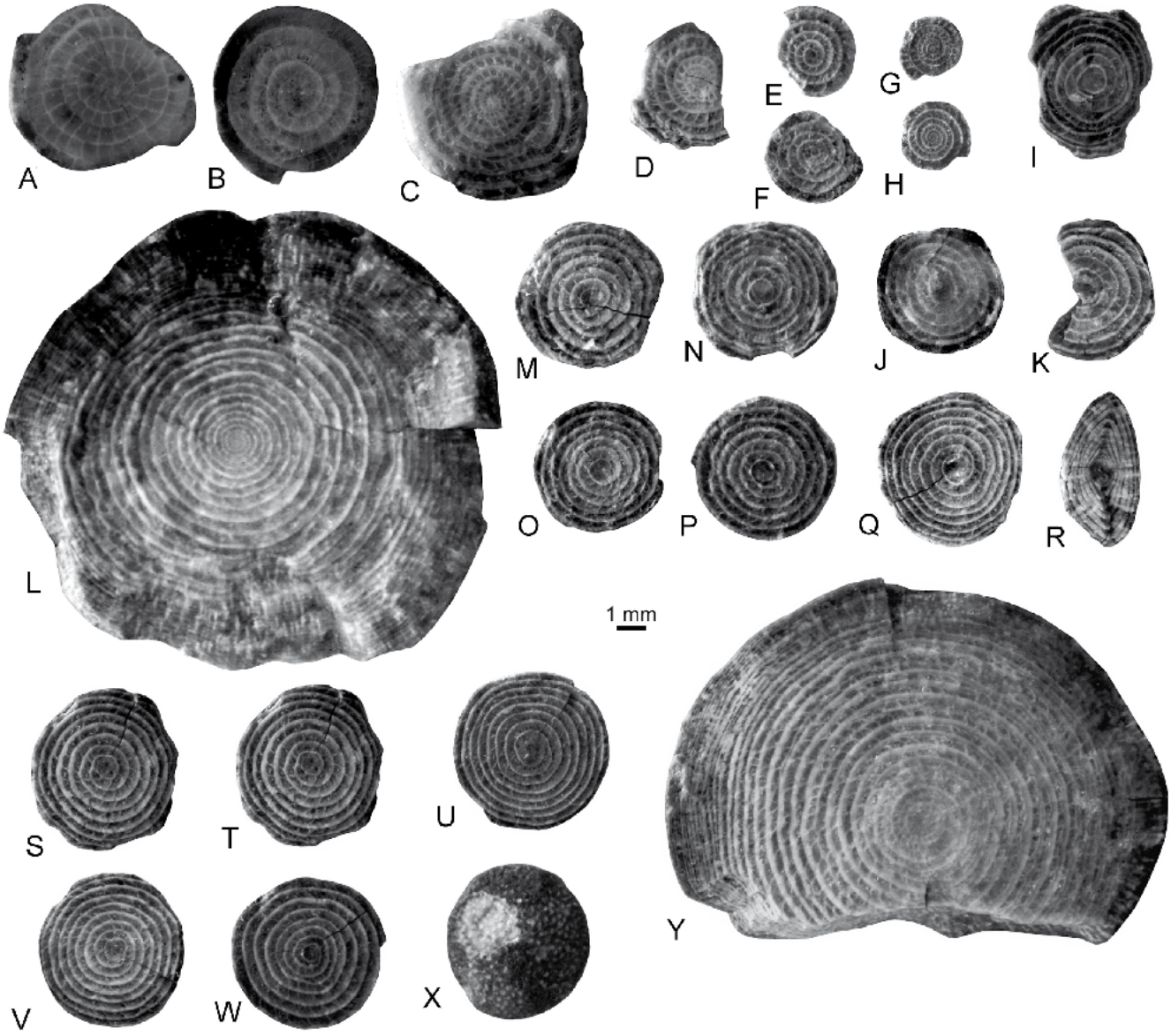

FIGURE 4. Key Larger foraminifera found along Las Bellostas section. A-B) Assilina laxispira DE LA HARPE, 1926 (megalospheric or A forms in equatorial sections); C-F) Nummulites rotularius DESHAYES, 1838 (C-D: microspheric or B forms; E-F: megalospheric or A forms, all in equatorial section); G-H) Nummulites beaumonti (megalospheric or A forms in equatorial sections); I-K) Nummulites tavertetensis REGUANT AND CLAVELL, 1967 (A or megalospheric forms in equatorial section); L-P) Nummulites crassus BOUBÉE, 1831 (L-O: megalospheric or A forms, P: microspheric or B form, all in equatorial section); Q-Y) Nummulites deshayesi D'ARCHIAC AND HAIME, 1853 (Q-X: megalospheric or A forms, all in equatorial section except 18 an axial section and X a test surface; Y microspheric or B form in equatorial section).

Paleomagnetic stability in Las Bellostas section

The occurrence of dual polarity pseudo-antiparallel ChRM vectors after restoration (restored mean inclinations are Normal: 40.5º [α_{95}; 12.5º] and Reversed: -43.3º [α_{95}; 8.1º]; Fig. 7) allows us to be confident about the primary character of the magnetization. The primary character is also supported by numerous magnetostratigraphic profiles very near Las Bellostas (Bentham and Burbank, 1996; Mochales *et al.*, 2012b; Rodríguez-Pintó *et al.*, 2013a; Vinyoles *et al.*, 2020; Fig. 2). Besides, the observed inclinations match very well with expected Paleogene inclinations obtained from hundreds of paleomagnetic sites in the Ainsa Oblique Zone (n: 114 Dec: 037.7º, Inc; 44.9º, α_{95}; 2.9º, k; 22.4, R: 0.9558) and in the External Sierras (n:222 Dec: 019.3º, Inc; 42.8º, α_{95}; 3.1º, k; 8.9, R: 0.8878) (Oliva-Urcia and Pueyo, 2019). However, due to the occurrence of local remagnetization records affecting part of the NW sector of the Balzes anticline (Santa Marina section Rodríguez-Pintó *et al.*, 2012b, 2013b), we have performed additional stability tests. A strict and rigorous

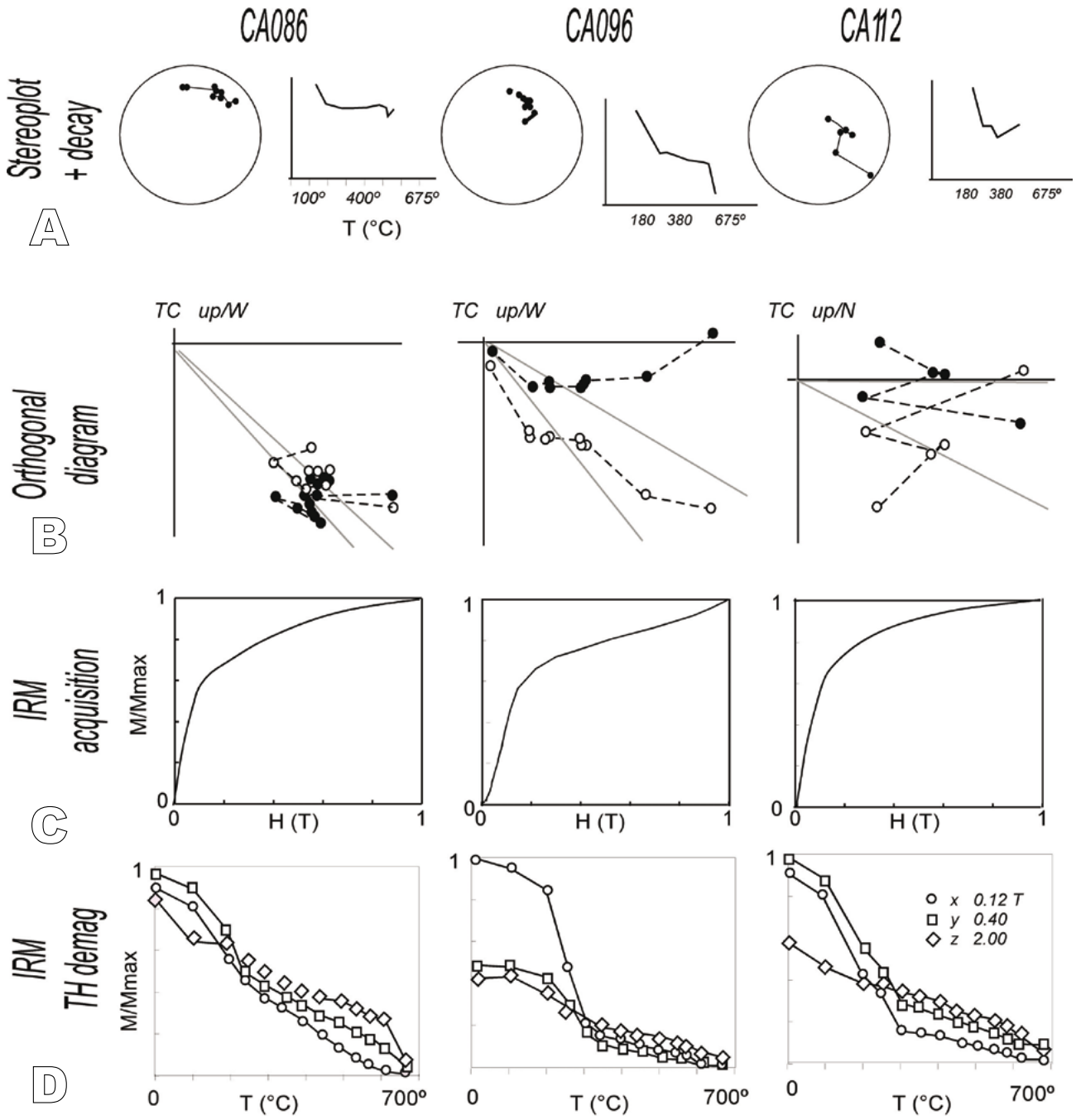

FIGURE 5. A-B) Stepwise thermal demagnetization and C-D) rock magnetism experiments. (A: decay curve and steronet; B: orthogonal diagram. Rock magnetism data of sister samples from selected sites in Las Bellostas section; C: IRM acquisition curves; D: three-axis IRM thermal demagnetization according to Lowrie (1990).

selection of first quality and reliable data in Las Bellostas section was based on the following criteria; only samples with Q≤2 and MAD<20º fitted with >3 steps were used in further calculations. Among other sources of noise, the occurrence of iron sulphides and the associated delays in the lock-in time (Larrasoaña *et al.*, 2004; Sagnotti *et al.*, 2005) may disturb the primary signal and accordingly, an additional filter based on the VGP paleolatitude was also considered (|VGP latitude|> 30°) and some few clear outliers were also removed.

Moreover, we have discretized las Bellostas section into 8 subsections (Bell-x) similarly to the processing carried out by Rodríguez-Pintó *et al.* (2008) in the

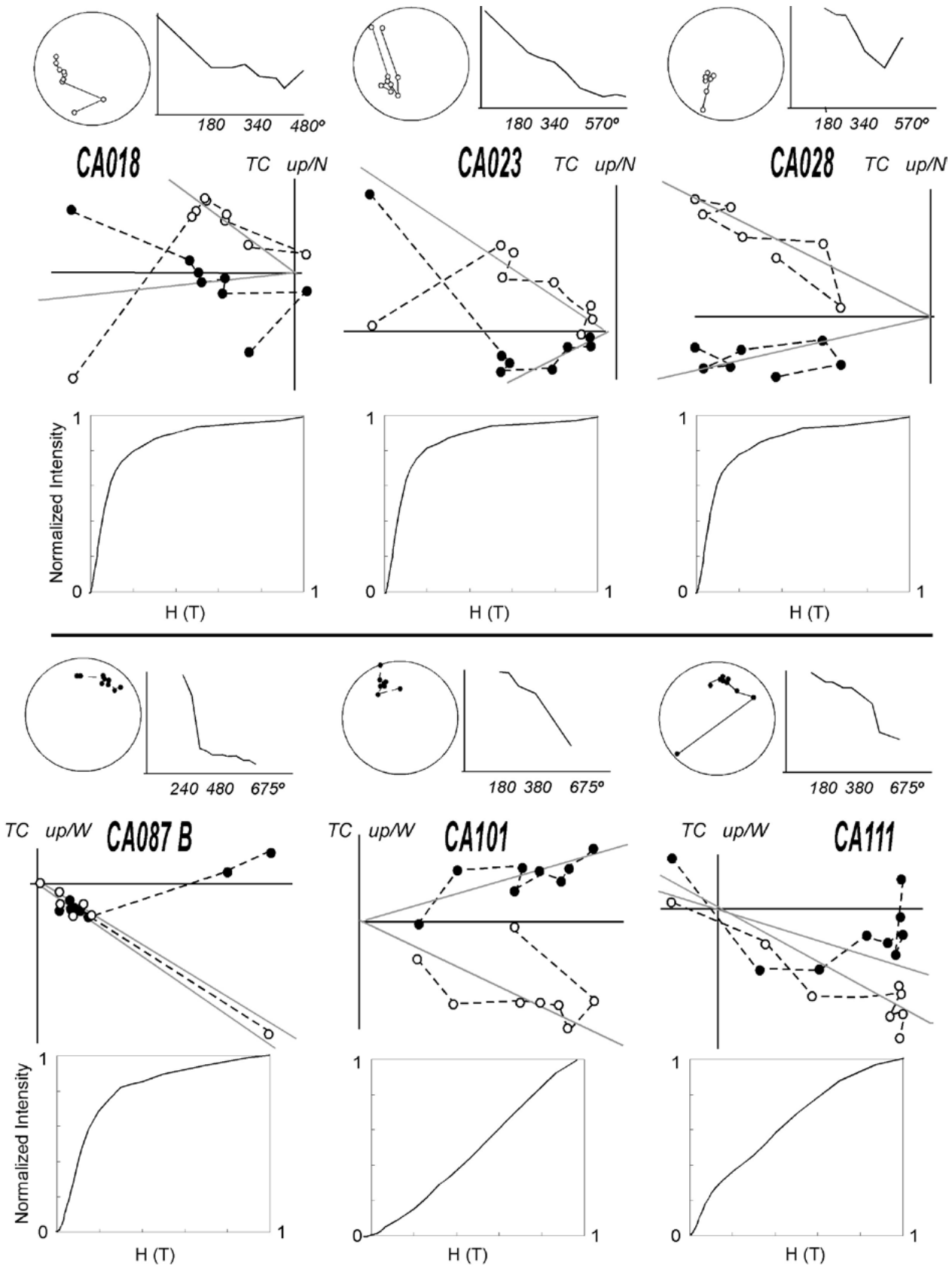

FIGURE 6. Demagnetization diagrams from selected Las Bellostas samples (CA-). For each sample stereographic projection of stepwise demagnetized vectors, intensity decay curves and IRM acquisition curves of sister samples are displayed (see Figure 5 caption).

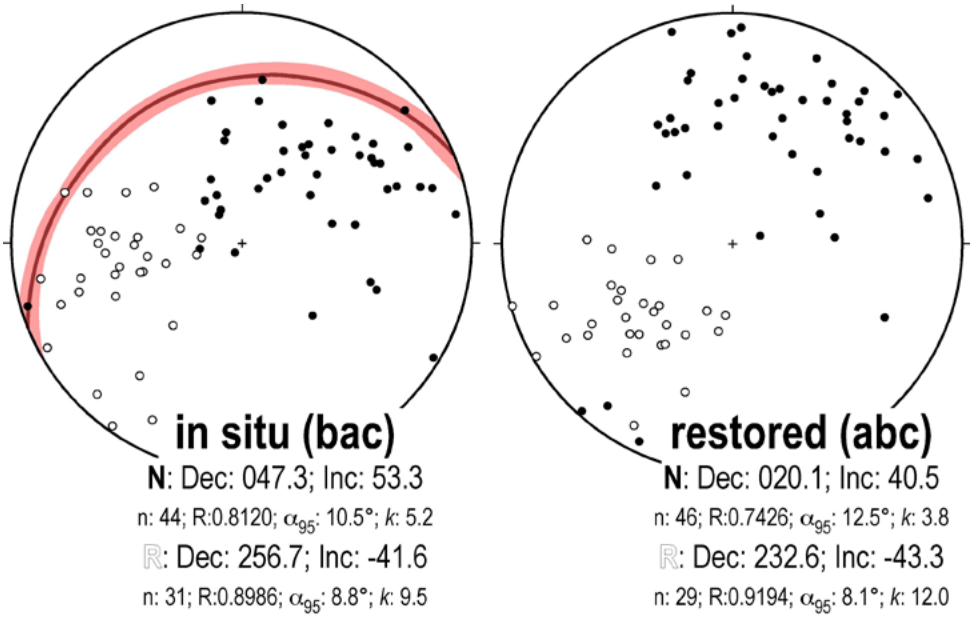

FIGURE 7. Mean paleomagnetic vectors (and Fisher's statistics) in Las Bellostas section (only Q1 and Q2 data were projected). A) before any correction (in situ-geographic coordinate system-bac). Bedding planes (large red circles) are also plotted. B) After bedding correction (paleogeographical reference system-abc).

Isuela section or the one by Mochales *et al.* (2012a) in the western limb of the Boltaña anticline (just to the East of Balzes anticline). Each subsection belongs to a single chron (except for BELL-1 and 5 due to their short duration or low accumulation rate), trying to get an even distribution along the stratigraphic thickness and its equivalent age (Table 2). Since the monotonous strike and dip in the sampled section precludes to carry out a significant fold test (Table 2) we have, therefore, involved additional standard paleomagnetic sites available in the northern sector of the Balzes anticline (Rodríguez-Pintó *et al.*, 2016, 2020) (Table 3).

Two different approaches gave comparable results (Fig. 8). On one side, the classic fold test by McFadden (1990) yielded a best fitting around 70-80% (f:0.4) unfolding (f:2.89 at 100%). On the other hand, the SCI estimates using the bootstrap approach (Calvín *et al.*, 2017) (deviation Ratio: 1.40, intersection Ratio: 0.73) based on 500 solutions (mean between 30 random pseudosamples) gave a mean of Dec/Inc: 051/50 (Kent ellipse zeta95: 15.7 [310, 8], zeta95: 11.03 ([214, 37]), k: 106.6, α_{95}: 0.6 and A/n: 4.93 and a similar mean unfolding percentage: 70% + -29% (optimal restoration ratios range from 34% to 114%) very similar to the standard small circle intersections (SCI) solution (Waldhör and Appel, 2006): Dec/Inc: 52º, 49º k: 200.2, α_{95}: 3.4 and A/n: 4.46, unfolding percentage: 73% + -27%. All these results are derived from the software VPD (Ramón *et al.*, 2017) with additional SCI implementations after Calvín *et al.* (2020).

The slight (and non-significant) deviation from the total restoration (≈20-25% remaining) of the beds in the classic fold test is similar to the one obtained in the SCI approaches. However, the SCI methods yield unfolding errors close to 30%, including the total restoration of the beds (paleohorizontal) and guarantee the primary character of the magnetization. As it will be shown later, the lack of total convergence of the ChRMs in the paleohorizontal is partially due to the syn-rotational character of the magnetization, and gives a "banana-like" scattering responsible for the artificial deviation of the stability tests (Pueyo *et al.*, 2016 and references therein). In conclusion, the above results provide support to a prefolding and primary character (age of magnetization= age of rocks) of the ChRM.

Local Polarity Sequence (LPS)

We have applied some quality criteria for the definition of local chrons; only directions with Q1 and Q2 were used (see Paleomagnetic directions section). Apart, some additional filtering criteria were applied to removed low-quality data; those that we applied to perform the stability tests (see previous sections). Finally, the robust polarity defined in the RIx sites (Rodríguez-Pintó *et al.*, 2016) distributed all along Las Bellostas section were taken into account for the construction of the Local Polarity Sequence (LPS). As a general rule the lower part of the section (below 280m) shows dominant reverse polarity while the upper part (550m) displays normal polarity. The middle portion is not so unambiguous. Therefore, and aiming to obtain a

TABLE 2. Mean paleomagnetic vectors (BELL-x subsections) derived from the discretization of Las Bellostas Local Polarity Sequence (LPS) data. Legend: Dec-BAC= declination before bedding correction. Dec-ABC= declination after bedding correction. Inc-BAC= inclination before bedding correction. Inc-ABC= inclination. Inclination and Declination also given together with standard statistical parameters (α95 and *k*). Age (polarity and chrons) derived from the correlation to the Geomagnetic Polarity Time Scale (GPTS) (Figure 10). Alt mean, mean stratigraphic height. Bedding dip. Strike and dip following the right-hand-rule (rhr)

Site	Long	Lat	Strike	Dip (rhr)	Age	Alt mean	n	Dec-BAC	Inc-BAC	α95	*k*	Dec-ABC	Inc-ABC	α95	*k*	Polarity	Chron
BELL-1	-0.01802669	42.34322367	247	30	43.42	18.27	11	257.4	-24.4	22.1	5.2	62.8	29.2	20.4	6.0	N+R	C20n-C20r
BELL-2	-0.01814095	42.34398763	246	30	42.15	61.71	7	261.1	-43.2	14.8	15.1	52	43.2	14.7	17.7	R	C19r
BELL-3	-0.01976893	42.34453898	246	30	41.68	123.17	6	274.8	-50.9	14	19.8	53.4	55.9	14.0	23.9	R	C19r
BELL-4	-0.02112727	42.34704765	245	33	40.60	241.50	6	251.6	-43.6	19.9	10.2	42.3	38.2	19.5	12.8	R	C18r
BELL-5	-0.02389279	42.34963134	242	33	39.72	411.36	11	53.9	51.6	23.1	10.2	25.9	38	20.7	5.4	N+R	C18n1-C18r1-C18n2
BELL-6	-0.02420470	42.35319229	244	33	39.38	574.91	11	51	39.5	12.2	14.9	30	27.3	12.3	14.7	N	C18n1
BELL-7	-0.02436014	42.35551058	246	28	39.16	675.45	11	41	60.2	19	6.7	12.9	40	19.6	6.5	N	C18n1
BELL-8	-0.02378122	42.35806957	243	26	38.85	818.17	12	40	55.6	18.4	6.5	16	40	18.4	6.5	N	C18n1

robust LPS, only two or more consecutive sites sharing the same polarity were considered to define a chron all along the profile.

The 950m Las Bellostas LPS is composed by eight magnetozones; from R1 to N4 (Fig. 9). The very bottom of the profile (site RI05) displays reverse polarity (R1) as well as the first sites of the profile (up to site 9). Then, a section with low paleolatitude values includes some consecutive normal polarity data (meters 23 to 42) has been considered as N1. From that point, the R2- R3 zone is very clear and reaches meter 285, although two consecutive normal sites around meter 170 allows us to tentatively define chron N2 (see further explanations later). From 285m to 378m, N3 is unambiguously defined and includes site RI03. Then, R4 is poorly defined in this part of the section (from 400 to 440m) but supported by the reverse polarity of site RI08 (8 samples). From that point onwards (up to 950m) the section is of normal polarity (N4).

DISCUSSION

Correlation to the GPTS

The correlation between las Bellostas LPS and the GPTS (Ogg, 2012) (Fig. 10) is based the local pattern of magnetozones, the biostratigraphic data introduced in this paper as well as the stratigraphic relationships with nearby sections with additional chronostratigraphic constraints. The age model provided is supported by:

i) The excellent outcropping conditions in the southern portion of the Jaca Basin that includes continuous, thick and

TABLE 3. Paleomagnetic sites in the Balzes region (all data by Rodríguez-Pintó *et al.*, 2016). See caption of Table 2 for abbreviations

Site	Strike	Dip (rhr)	Age	Alt mean	n	Dec-BAC	Inc-BAC	Dec-ABC	Inc-ABC	α95	*k*	Polarity	Chron
RI01	259	23	39.12	618.00	13	4	55	359	32	18	6	N	C18N1N
RI02	256	24	39.92	497.00	10	31	75	4	54	15	12	N	C18N2N
RI03	265	38	41.27	335.00	3	36	46	23	14	13	133	N	C19N
RI04	247	24	41.40	164.00	11	243	-50	38	43	7	44	R	C19R
RI05	258	32	42.25	0.00	10	264	-54	45	46	14	15	R	C19R
RI06	264	34	42.00	22.00	11	274	-27	76	27	15	12	R	C19R
RI07	259	32	41.70	134.00	11	256	-54	41	42	4	128	R	C19R
RI08	275	46	40.65	400.00	8	242	-48	41	15	17	13	R	C18R
RI09	247	25	37.36	860.00	7	9	67	354	44	29	6	N	C17n.1n
DA01-DBA01	200	40	40.65		63	249	-20	48	45	5	15	R	C18R
SS01	7	40	43.43		10	170	-50	36	45	12	33	R	C20R
SS02	12	81	43.93		11	146	-33	49	41	8	104	R	C20R
SS03	13	51	44.43		12	192	-63	69	34	6	58	R	C20R
SS04	5	43	44.93		11	208	-73	73	38	5	114	R	C20R
SS05	5	36	45.43		21	227	-61	70	31	10	14	R	C20R
SS06	8	41	45.72		17	207	-59	63	33	6	35	R	C20R

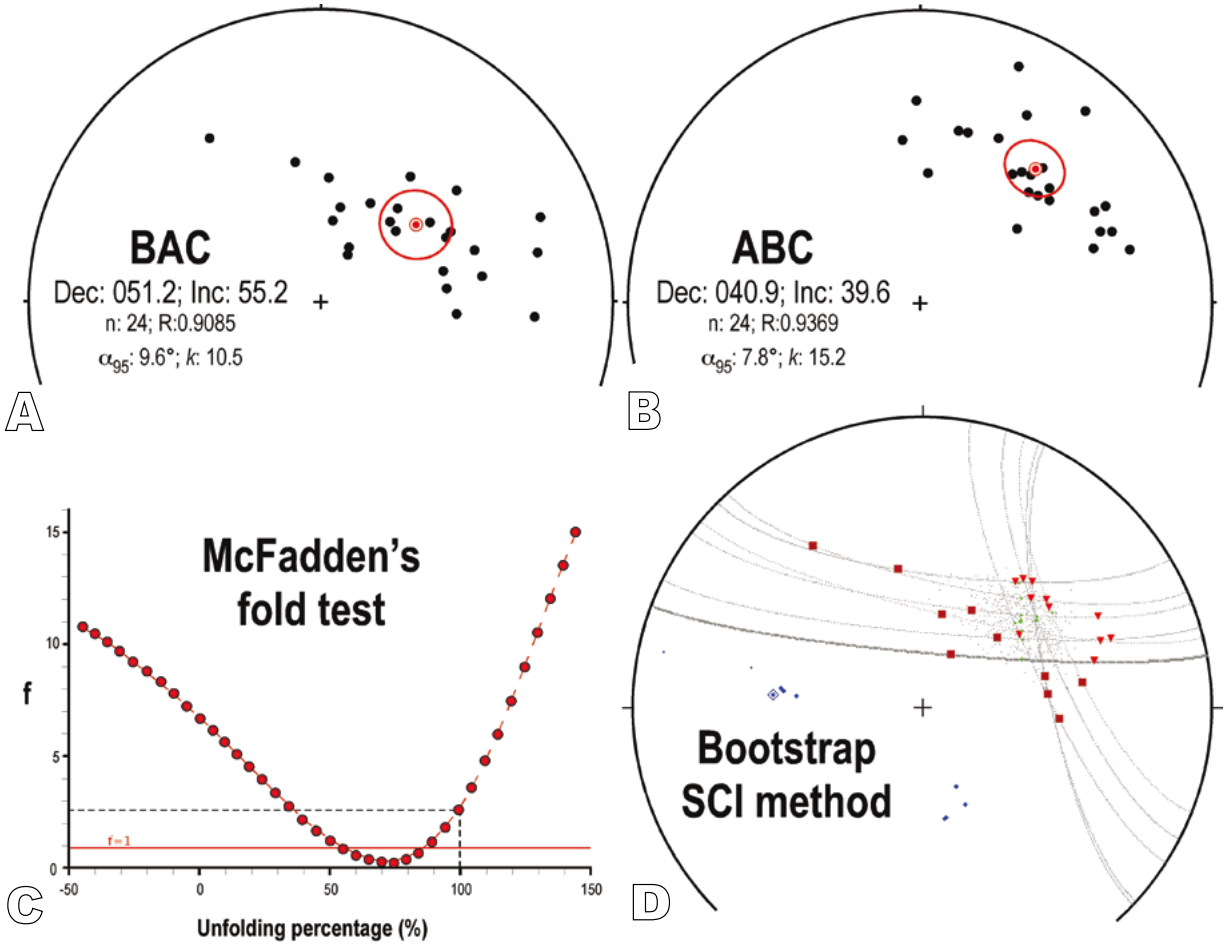

FIGURE 8. Paleomagnetic stability. A-B) Stereographic projection of paleomagnetic site means in the Balzes region (Rodríguez-Pintó *et al.*, 2020) including Bell-x sites derived from the discretization of Las Bellostas section (Table 2). All vector means projected in the lower hemisphere. C-D) paleomagnetic tests in the northern sector of the Balzes anticline run under the Virtual Paleomagnetic Directions (VPD) software (Ramón *et al.*, 2017). C: evolution of the "f" parameter by McFadden (1990) during progressive unfolding (0% in-situ vectors and 100% after total restoration). D: Small circles intersection technique (bootstrap approach after Calvín *et al.*, 2017).

long stratigraphic sequences from Lutetian to Priabonian times. This fact is supported by the detailed cartographic work in the region (Puigdefàbregas, 1975; Montes-Santiago, 2002, 2009) that allows for reliable stratigraphic correlations among the sections (Fig. 11).

ii) The existence of several and long nearby magnetostratigraphic studies (Fig. 2); the Arguis-Monrepós section (Hogan, 1993; Hogan and Burbank, 1996; Kodama *et al.*, 2010), the Isuela section (Rodríguez-Pintó *et al.*, 2012b). Additional preliminary data to the East include the Belsué section (Garcés *et al.*, 2014; Valero *et al.*, 2020) as well as the Santa Marina and the Gabardiella sections (Rodríguez-Pintó *et al.*, 2012a and 2017 respectively).

iii) Apart from Las Bellostas section, nine previous paleomagnetic sites (RI-) located along the Isuela riverbanks were also considered for the calibration (Figs. 10; 12). Besides, seven closer sites from Lutetian marls in the eastern flank of the anticline (DA01 and SS-x sites) were also taken into account (Rodríguez-Pintó *et al.*, 2016). Finally, the polarity from eleven additional paleomagnetic sites (US- and NT- sites by Pueyo, 2000 and Pueyo *et al.*, 2003) located between the Arguis-Monrepós and Las Bellostas sections were also used to reinforce the magnetic correlation eastwards.

The reverse polarity found at RI05 (very base of the profile) is located within the Boltaña Fm. and supported by larger foraminifera belonging to the SBZ11 (sample BA07), thus it has been correlated to C22r chron (Fig. 10) in agreement with previous data (Ara and Bal Ferrera sections by Mochales *et al.*, 2012b and San Pelegrín one by Rodríguez-Pintó *et al.*, 2013a). Samples BA04, BA05 and BA06 contain larger foraminifera assemblages belonging to the SBZ15 indicating a late Middle Lutetian age. Given the normal polarity of the corresponding paleomagnetic sites (N1) found in the lower samples (samples BA05 and BA06)

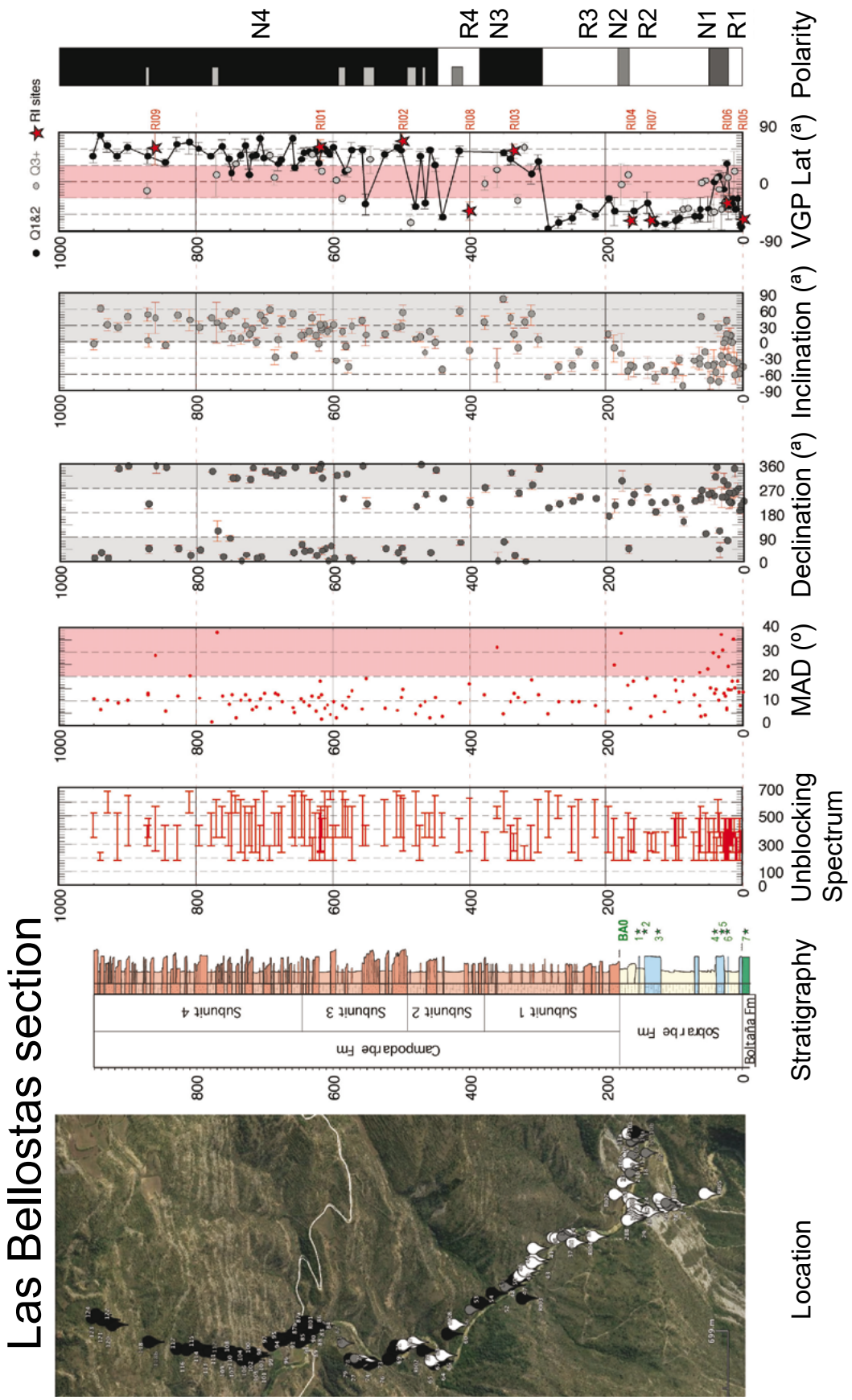

FIGURE 9. Local polarity sequence in Las Bellostas section. From left to right; Location on the satellite picture with indication of the magnetic polarity and the number of site, Stratigraphy; column and location of biostratigraphic (BA0-) samples. Characteristic Remanent Magnetization (ChRM) data: Unblocking spectrum (minimum and maximum temperature in ºC), Maximum Angular Deviation (MAD in º), Declination, Inclination, and corresponding Virtual Geomagnetic Poles (VGP) latitude and derived polarity of the ChRM.

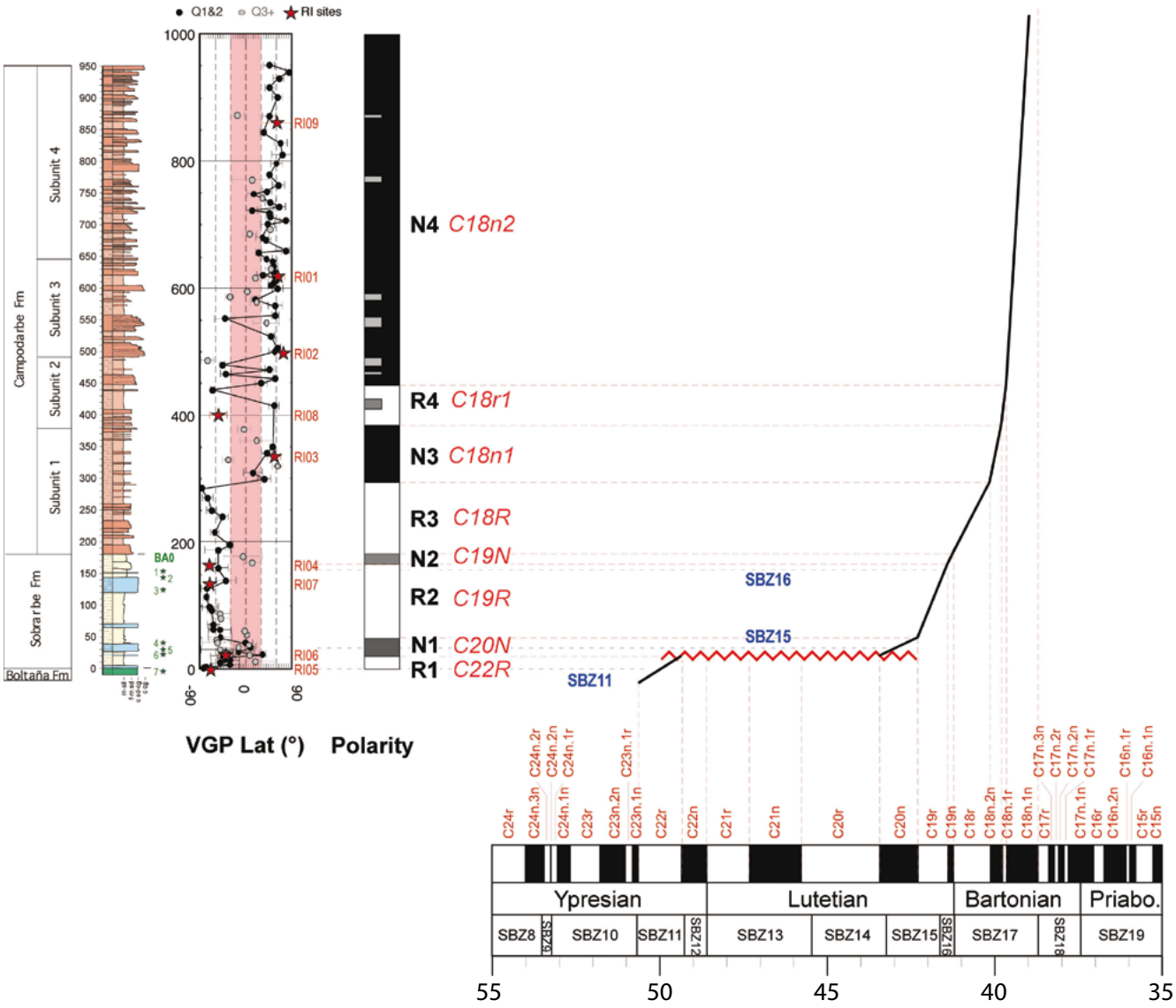

FIGURE 10. Las Bellostas Local Polarity Sequence (LPS) correlation to the Geomagnetic Polarity Time Scale (GPTS) of Ogg (2012).

and the occurrence of upper samples with reverse polarity (sample BA04) we have correlated these levels around chrons C20n and C19r, and the upper most sample (sample BA04 with larger foraminifera belonging to the SBZ15 as well) would correlated to C19r. The unconformity between the Boltaña Fm. and the Upper Guara Mbr., precludes the record of chrons C22n to C20r. This sedimentary hiatus is longer than in other closer sections (Gabardiella or Isuela; Barnolas *et al.*, 2019) due to its structural position, *i.e.*, because the profile is located at the hinge of the Balzes anticline, and due to the syntectonic character of the Guara Fm. (Barnolas and Gil-Peña, 2001; Rodríguez-Pintó *et al.*, 2016). The location of samples BA02 and BA03 at the top of the marine deposits (around 170m of the log, Fig. 3) together with their unambiguous biostratigraphic affinity to SBZ16 and the occurrence of a poorly define normal polarity zone (N2) atop these samples allow us to pin this interval in chron C19r (and N2 as C19n). The following 100m of section with a dominant and robust reverse polarity record (R3) is then correlated to the base of Bartonian (C18r). It is worth mentioning the continental caracter of this part of the section (Campodarbe Fm.), which is laterally equivalent to the Arguis marls, was already pointed out by Puigdefàbregas (1975) and Montes-Santiago (2002), and also implies that the lower continental deposits of the Campodarbe Fm are much older at Las Bellostas than in the western part of the Jaca Basin.

The Arguis-Monrepós (Hogan and Burbank, 1996) section and the aforementioned stratigraphic works are key

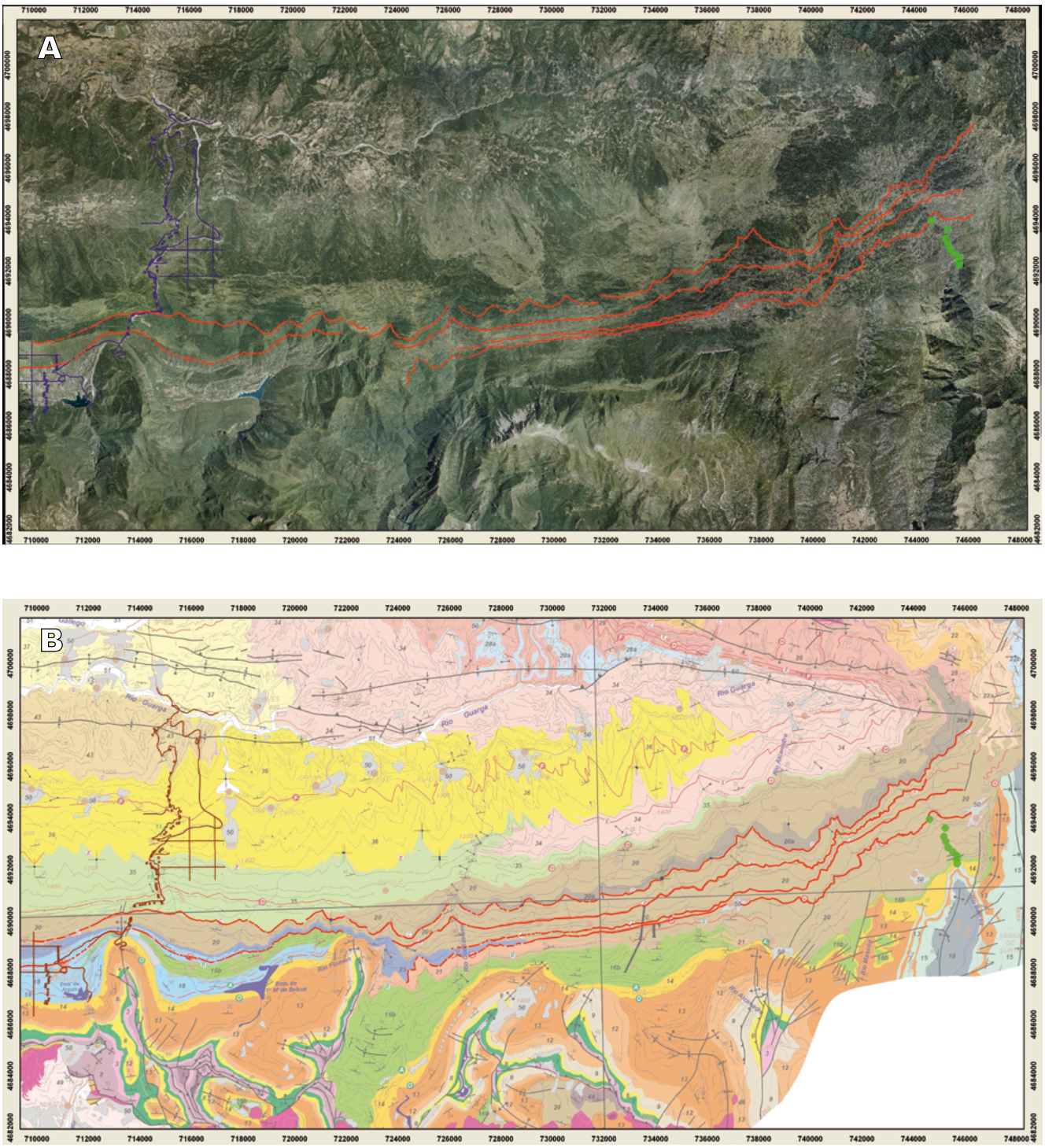

FIGURE 11. Geological map of the Eastern Jaca Basin by Montes-Santiago (2009) supporting the correlation between Las Bellostas (this study) and Monrepós-Arguis (Hogan, 1993) and Isuela (Rodriguez-Pintó *et al.*, 2012a) sections. Several NTx and USx paleomagnetic sites (Pueyo *et al.*, 2003) and their magnetic polarity (black is normal and white is reversed) are also shown to support the correlation. Geographic Information System (GIS) from Rodríguez-Pintó (2013).

for building up the age model atop Las Bellostas section as well as for estimating the age of the paleomagnetic sites used to calculate the rotation velocity (see next section) (Fig. 12). That section represents 3700m thickness and starts just at the top of the Guara limestones, crosses the Arguis (1.000m) and Belsué-Atarés deltaic formation (175m) and reaches the top of the Campodarbe fluvial deposits, 2500m above the top of the marine sequence. These authors studied 121 different stratigraphic levels. The Arguis section was revisited by Kodama *et al.* (2010)

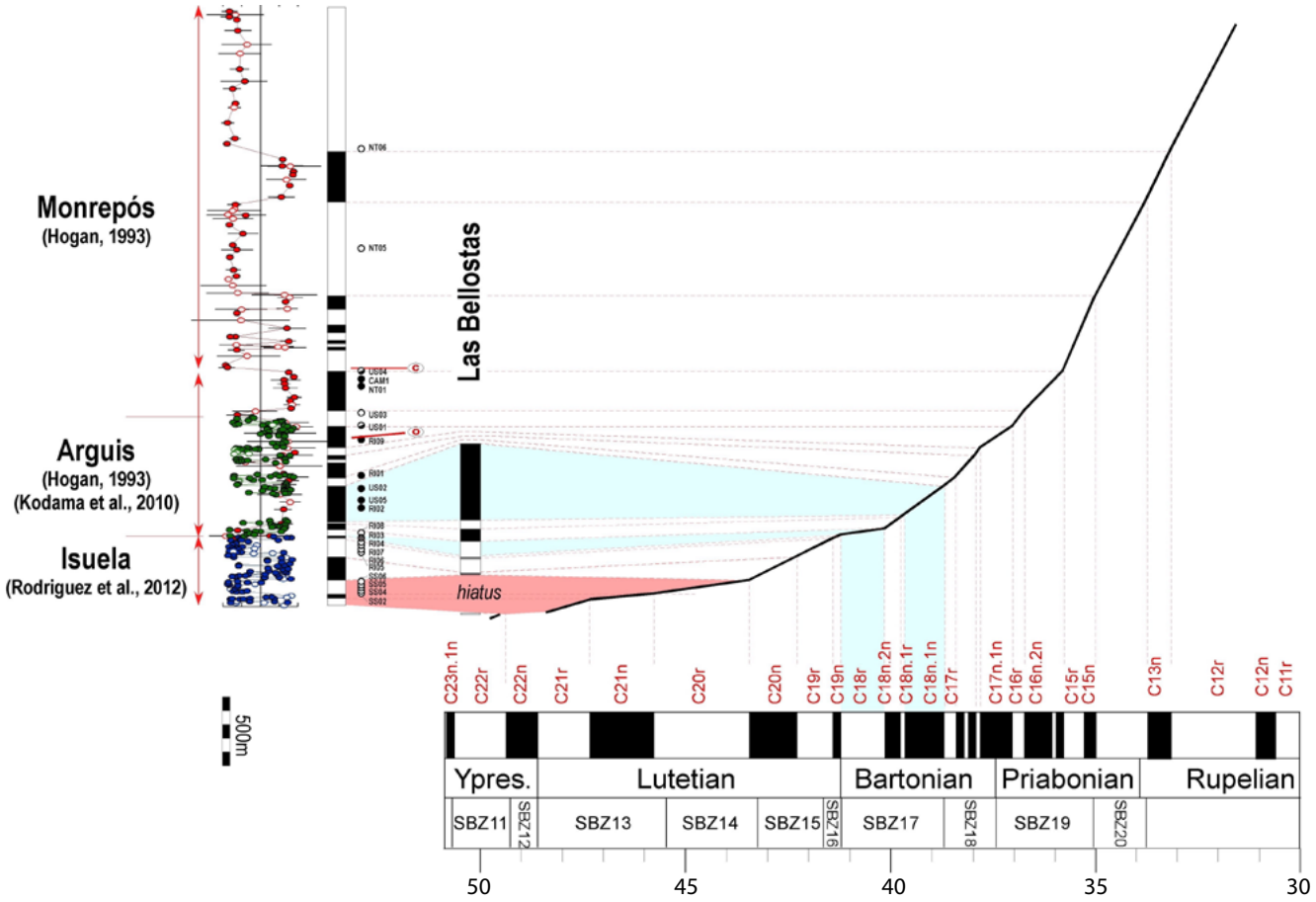

FIGURE 12. Correlation between Las Bellostas and Monrepós-Arguis-Isuela sections of the eastern Jaca Basin (Hogan, 1993; Kodama *et al.*, 2010; Rodríguez-Pintó *et al.*, 2012a) and the Geomagnetic Polarity Time Scale (GPTS) (Ogg, 2012). Intermediate polarities derived from previous standard paleomagnetic sites (Pueyo *et al.*, 2003) are also included as well as referencebeds (red "O" and "C") identified by Montes-Santiago (2009).

to improve the resolution of the Bartonian magnetozones and recently reinterpreted by Garcés *et al.* (2020). Besides, the underneath Guara Fm. was entirely studied and recalibrated by Samsó *et al.* (1994) and Rodríguez-Pintó *et al.* (2012a) in the Isuela section (520m). Costa *et al.* (2010) and Garcés *et al.* (2020) have modified the dating of the Belsué top considering also long sections from the eastern Pyrenean foreland basin that suggest a synchronous closure of the marine gateway with the Atlantic during the middle Priabonian (C16n.2n) in agreement with previous planktonic foraminifera and charophyte biostratigraphic data (Canudo *et al.*, 1988; Canudo and Molina, 1992) and confirmed latter with larger foraminifera (Molina *et al.*, 2013). This interpretation is also supported by preliminary data in the eastern flank of the Pico del Aguila anticline (Belsué section by Garcés *et al.*, 2014; Valero *et al.*, 2020).

This reviewed age model for the eastern Jaca Basin (Fig. 12) correlates the base of Guara Fm. with C21r and its top to C19n (Lutetian/Bartonian boundary). The Arguis marls span along the Bartonian and part of the Priabonian (C18 to C16n1n) depending on the along-strike position because of the progradation of deltaic facies (Belsué-Atarés Fm.). It seems clear that the Guara limestones could even reach chron C18r (Rodríguez-Pintó *et al.*, 2019) as it has been demonstrated in the western sectors (Silva-Casal *et al.*, 2019, 2021). The top of the Belsué-Atarés was re-assigned to the top of C16n1n (Costa *et al.*, 2010; Garcés *et al.*, 2020). The base of Campodarbe Fm in the Monrepós section starts at C15r and the isolated normal chron found around meter 3000 fits with C13n (Fig. 12). Two distinct beds (namely "0"and "C" in Figs. 11; 12) described and mapped by Montes-Santiago (2002 and 2009) fall within the Arguis-Monrepós section and have been tracked to the eastern part of the Jaca molasse basin where Las Bellostas section is located. Bed "0" has an equivalent age to chron C17n.1n and bed "C" falls within chron C15r. Since bed "0" is atop the upper most part of Las Bellostas and the upper 550m of this section displays a dominant normal polarity (N3, R4 and N4) we have

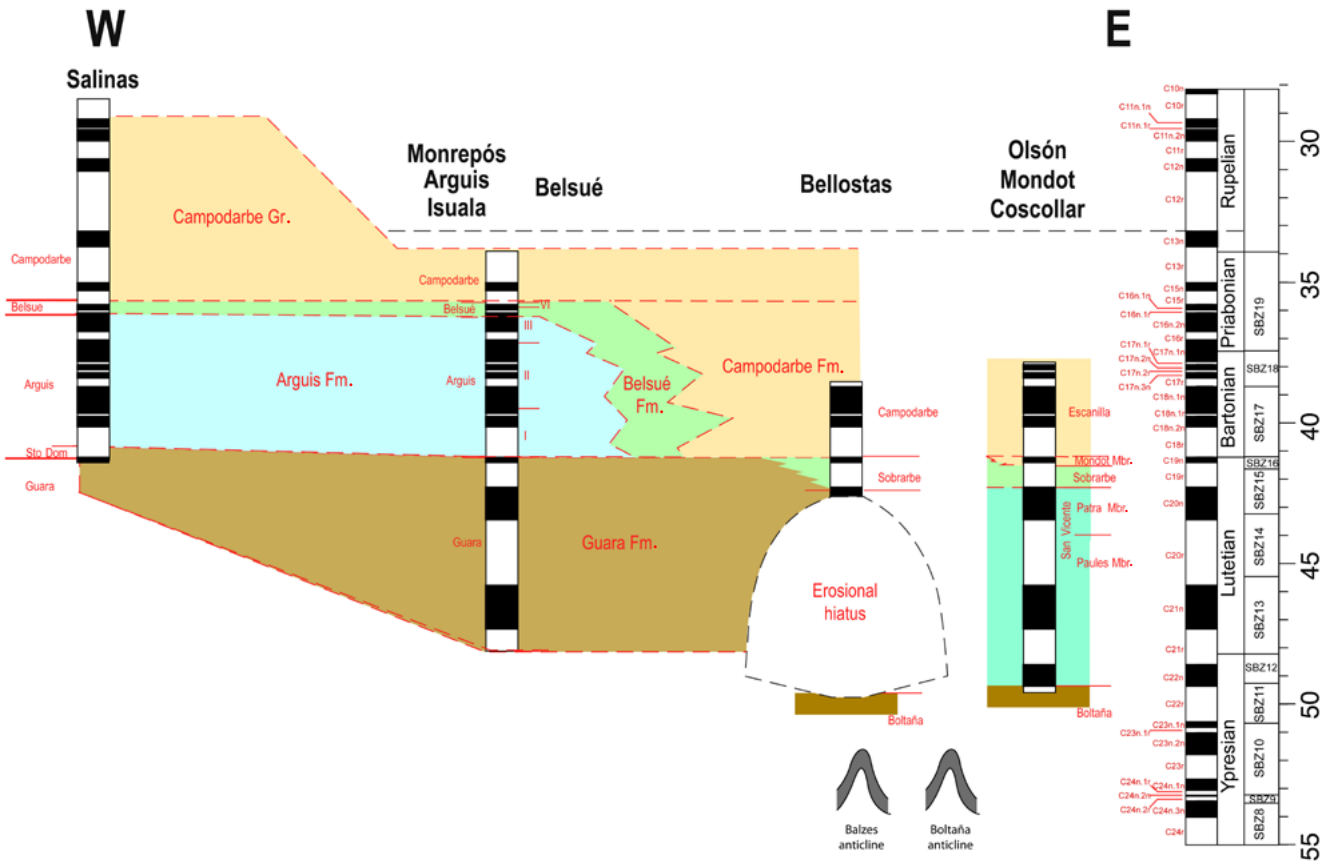

FIGURE 13. West to East correlation panel (drawn to geological time) of the eastern Jaca Basin integrating all available magnetostratigraphic sections (gray rectangles). See location of sections in Figure 3. Geomagnetic Polarity Time Scale (GPTS) according Ogg (2012).

correlated this interval with chrons: C18n.2n, C18n.1r and C18n.1n respectively.

This age model (Fig. 12) allows the dating of the standard paleomagnetic sites located in the Balzes anticline and in the northern sector of the Guara massif (Table 3 and Rodríguez-Pintó *et al.*, 2016). RIx sites can be now precisely dated within the age model of Las Bellostas (Fig. 10) since they are located along that section. US01 and US03, NT01 and CAM1 (Pueyo *et al.*, 2003) must fall within the lower part of C16 chron, while NT05 and NT06 (the youngest sites) would correspond to C13r and C12r respectively, according to the Monrepós section (Hogan and Burbank, 1996). At the eastern flank of the Balzes anticline (SS- sites), the mudstones in the lower part of the section must belong to the C20r chron according to the chronostratigraphic frame in the Coscollar section (Ainsa Basin) by Mochales *et al.* (2012b). This chronostratigraphic frame allows us to analyze the relationships between the age and the vertical axis rotation observed in the paleomagnetic data and thus, to determine the rotation age and velocities of the underneath thrust sheets (Balzes-Boltaña after Millán, 1996).

Implications for the chronostratigraphy of the Eastern Jaca and Western Ainsa Basins

The chronostratigraphic results obtained in Las Bellostas section are in agreement with published magnetostratigraphic sections in the Ainsa Basin (Mochales *et al.*, 2012b; Vinyoles *et al.*, 2020) and in the Jaca Basin (Garcés *et al.*, 2020; Rodriguez-Pintó *et al.*, 2012a; Vinyoles *et al.*, 2020). Nevertheless, some remarks are needed to explain the complexity of the regional tectonic and sedimentary setting (Fig. 13).

In addition to the erosional unconformity, below the Sobrarbe Fm., which has previously been reported (Barnolas and Gil-Peña, 2001; Rodríguez-Pintó *et al.*, 2016), some additional considerations are here outlined. The onset of the Sobrarbe Fm., including the basal limestone bed, takes place in the uppermost part of C20n (within SBZ-15) as it happens in the Coscollar and Mondot sections (Ainsa Basin) (Mochales *et al.* 2012b). This age is older than the boundary age between the Middle and the Upper Guara Mbrs., defined in the Isuela Section (Rodríguez-Pintó *et al.*, 2012a). The uppermost beds of the Sobrarbe Fm. fall

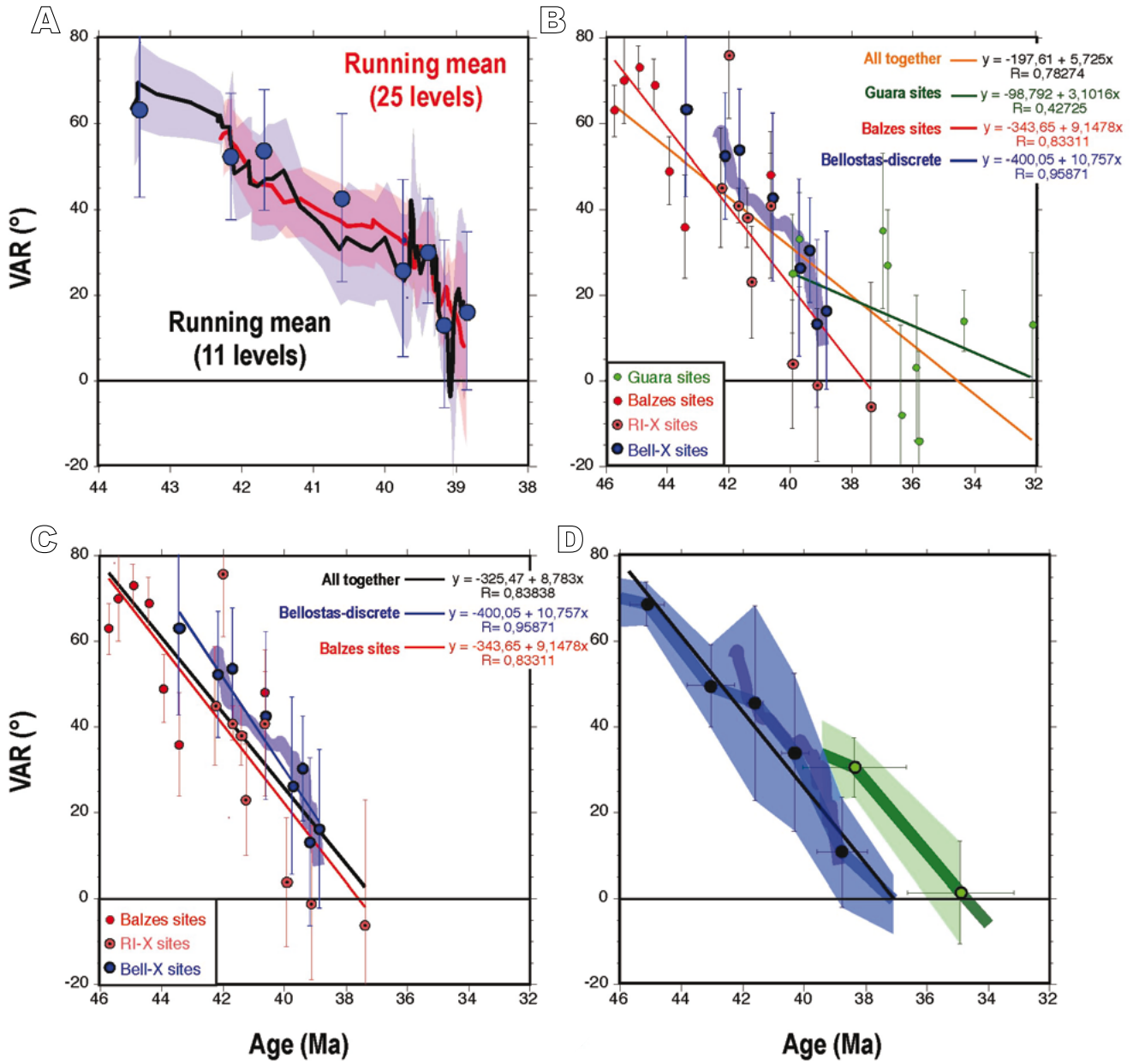

FIGURE 14. Rotation velocity deduced from paleomagnetic data in Las Bellostas section and surrounding area (northern sector of the Balzes anticline). A) Las Bellostas running averages (11 and 25 levels). B) Discrete data; Bell-x sites and data from the northern sector of the Balzes anticline (Rodríguez-Pintó *et al.*, 2016) and the Guara system (Pueyo *et al.*, 2003). C) Data from the Balzes anticline alone. D) Robust averages in the Balzes (blue) and Guara (green) thrust sheets.

within C19n, within SBZ-16. In the Ainsa Basin sections, the C19n stands inside the transitional facies (Mondot Mbr.) of the Sobrarbe delta complex (Dreyer *et al.*, 1993; Kjemperud *et al.*, 2004) that attain the C18r (Mochales *et al.*, 2012b). In the Isuela section, the upper beds of the Upper Guara member also are in the C18r (Rodríguez-Pintó *et al.*, 2019). The older age found for the uppermost beds of the Sobrarbe Fm., in the Las Bellostas section, is due to erosion below the Campodarbe Fm. unconformity. In the Eastern External Sierras, the lower boundary of the Upper Guara Mbr. coincides with a growth unconformity, and the lateral relationships between the Upper Guara Mbr. and the Sobrarbe Fm. are well constrained. However, in the western External Sierras (Isuela section), where the Upper Guara Mbr. was defined (Samsó *et al.*, 1994), its lower boundary is significantly younger (inside C19r) (Rodríguez-Pintó *et al.*, 2012a). In consequence, no exact age equivalence between Upper Guara Mbr. and Sobrarbe Fm. is supported accordingly with the original definitions.

The base of the Campodarbe Fm in Las Bellostas section is C18r and, as described before, is sharp and probably

slightly unconformable following the complex stratigraphic relationships around the Cambodarbe unconformity in the Boltaña anticline (Mochales *et al.*, 2016; Montes-Santiago, 1992, 2009; Puigdefàbregas, 1975). The studied lower part of the Campodarbe Fm., in Las Bellostas section (770m in total), belongs to C18 (Bartonian). In the Olsón section (Ainsa Basin) studied by Vinyoles *et al.* (2020), the C18 corresponds to the lower 450m, including part of the Mondot and Olson Mbrs. (Escanilla Fm.) of Dreyer *et al.* (1993). In the Guarga synclinorium, three sections with an accurate chronostratigraphy (see Vinyoles *et al.*, 2020) permit comparison with data obtained in Las Bellostas section. These are, the Yebra de Basa section (Hogan and Burbank, 1996; Oms *et al.*, 2003 and Vinyoles *et al.*, 2020), the Belsué section (Garcés *et al.*, 2014 in Vinyoles *et al.*, 2020), and the Arguís-Monrepós section (Costa *et al.*, 2010; Hogan and Burbank, 1996; Kodama *et al.*, 2010) (Fig. 2). In all these sections, the age-equivalent beds to the Campodarbe Fm. represented in Las Bellostas are in marine (prodeltaic to deltaic) facies in a stratigraphic relationship well-known since Soler and Puigdefàbregas (1970) and Puigdefàbregas (1975). As reflected in Vinyoles *et al.* (2020), significant variations in sedimentation rate occurred between them. Outlining only on the C18, which corresponds to the studied interval in Las Bellostas section, the Yebra de Basa section reports the highest sedimentary thickness with >1200m in a sedimentary succession including, from down to top, the Larres marls, the Sabiñánigo sandstone deltaic facies, the Pamplona marls and the Belsué–Atarés deltaic facies in transition to Santa Orosia conglomerates (Vinyoles *et al.*, 2020). In the Arguis–Monrepós section (Hogan and Burbank, 1996, reinterpreted by Costa *et al.*, 2010) and in the Belsué section (after Vinyoles *et al.*, 2020), both belonging to the southern limb of the Guarga synclinorium and representing the lower interval of the prodeltaic Arguis marls, the sedimentary thickness is significantly lower (≈500m). The resulting chronostratigraphy, thickness variations and lateral facies changes are in agreement and reinforce previous interpretations on the lower part of Campodarbe Fm. (Bibán facies) (Puigdefàbregas, 1975) and on the Escanilla Fm. (Dreyer *et al.*, 1993), with a progradation pattern that turns from an initial E to W to a latter N to S direction. Differences in thickness between the Olsón and Las Bellostas section (C18) can be explained by their distinctive structural position, with less accommodation space in Olsón, which is also reflected in the geometries of the fluvial sequence (more facies amalgamation and channel incisión in the Olsón profile).

Rotational kinematics of the Balzes anticline (Eastern External Sierras)

The magnetostratigraphic study (continuous log) undertaken from Las Bellostas section was aimed to characterize the VAR evolution of the Balzes anticline. As previously explained for the building of the LPS, we applied several objective criteria to reduce the noise (|VGP|>20º, MAD<20º, steps >3, only Q≤2); 60% of the data passed this filtering. For the rotation dating we have also involved the Bell-x subsections (Table 2), whose study was previously performed by Mochales *et al.* (2012b) and Rodríguez-Pintó *et al.* (2016). Except for the base of the profile where the accumulation rate is very low (<35m/Ma) and the time span is larger (Bell-1), the rest of the Bell-x subsections averages out time gaps around 0.5 (±0.2)Ma. Finally, we performed running averages of fisherian means all along the section (two different windows of 11 and 25 levels) (Fig. 14A). The age for every specific level is estimated from the age model (Fig. 10) assuming a constant accumulation rate during the chron duration. Considering Las Bellostas data alone, the rotation magnitude diminishes from the base (43.5Ma) to the top (39Ma) of the profile at an approximately constant rate (linear fit at 10.8º/Ma with R: 0.9587) from 60º clockwise (CW) to non-significant values.

Further data available from the Balzes anticline (Table 3) RI-, SS- and DBA sites (Rodríguez-Pintó *et al.*, 2016, 2020) and data from the northern Guara system (NT- and US- by Pueyo *et al.*, 2003) (Fig. 14B) are included in this study to check the consistency of this fitting. The Guara thrust sheet dataset spreads out in a large area, hardly covers the entire rotational period and therefore does not represent a reliable record of the rotational activity of the western thrust sheets except for its cessation during Priabonian times. Therefore, we here recommend revisiting this region in future studies. In any case, the entire dataset located in the Balzes thrust sheet (Fig. 14C) displays a much more robust and reliable characterization of its rotation history than before (Rodríguez-Pintó *et al.*, 2016). On one hand the RI- sites fit well with Las Bellostas records and on the other, the older data (SS- sites) give us a more complete temporal record of the rotational evolution of the system. Finally, we have merged all data together (Tables 2; 3) and we have estimated robust VAR means averaged out in time windows (Fig. 14D). These windows span from 45Ma to 35Ma and the Balzes and Guara thrust sheets have been processed separately (Table 4).

Focusing on the Balzes sheet, there is a continuous and consistent decrease of the rotation activity of this thrust sheet from 70ºCW, at least, from middle Lutetian (chron C20r, ≈45Ma) until the upper Bartonian/lower Priabonian (chron C17 s.l., ≈37-38Ma) when the rotational movement fully vanished. The rotation velocity seems to be constant and ranges around 9º to 11º/Ma (with R between 0.8331 and 0.9587).

Isochrony or diachrony of the South Pyrenean rotational movements

The rotation ages and historical pace obtained in the Balzes anticline are much more robust and coherent than

the data previously published by Rodríguez-Pintó *et al.* (2016) and allow for a comparison with the rotational kinematics of other well-known South Pyrenean structures (Figs. 15; 16), *i.e.* Pico del Aguila (Pueyo *et al.*, 2002; Rodríguez-Pintó *et al.*, 2008), Boltaña (Mochales *et al.*, 2012a; Muñoz *et al.*, 2013) and Santo Domingo anticlines (Pueyo *et al.*, 2021).

The diachrony related to the South Pyrenean thrust activity is long known and is reflected in the sedimentary record, particularly during the emplacement of the Gavarnie thrust sheet (Barnolas and Gil-Peña, 2001; Labaume *et al.*, 1985; Millán *et al.*, 2000; Muñoz *et al.*, 2013). Pioneer paleomagnetic data already supported the hypothesis of a rotational activity in the External Sierras front (Pueyo *et al.*, 1997). The rotation magnitudes deduced in these studies were still variable, both in time and space, being generally younger in the western sectors, in agreement to thrust kinematics. The occurrence of "articulation structures" was invoked in these pioneer studies to separate areas experiencing rotational processes from those non-rotated, and in order to explain the diachrony and the westward migration of the rotation mechanism. These structures would undergo compressions and extensions oblique to the regional stresses, avoiding severe space problems caused by the rotation, and should be geometrically oblique to the general Pyrenean structural trend. Later, the accomplishment of additional rotational kinematic data in the eastern oblique anticlines, *i.e.*, the Pico del Aguila, Boltaña, Balzes and Mediano anticlines by Pueyo *et al.* (2002), Mochales *et al.* (2012a) and Rodríguez-Pintó *et al.* (2008, 2016) questioned this initial hypothesis, since the main rotational event found in these structures was approximately coetaneous (Bartonian-Priabonian) in all of them, but, somehow independent of the folding and thrusting activity (Rodríguez-Pintó *et al.*, 2016).

Right after, Muñoz *et al.* (2013) reopened the scientific debate and proposed two main rotational periods. The first is coincident with the onset of the contractional deformation in the Gavarnie thrust sheet, which is not synchronous and thus, affects the structures as a function of their along-strike position (westward is younger). An average out of 45º and 55ºCW rotation is attributed to this period during the development of the Boltaña and Mediano anticlines respectively. The second, more moderate event (10-20ºCW) is proposed to encompass Priabonian to Oligocene times, and is in relation to the underthrusting of the Guarga basement unit below the Ainsa and Jaca Basins. This was witnessed by the remagnetized data obtained in the Internal Sierras (Oliva-Urcia and Pueyo, 2007; Izquierdo-Llavall *et al.*, 2015) and the southward transport of Mesozoic and Paleogene cover units in the External Sierras.

Finally, some additional data have been recently published. In the eastern sector, Beamud *et al.* (2017) have reported new pilot data in the Mediano anticline, while Pueyo *et al.* (2021) have published a complete

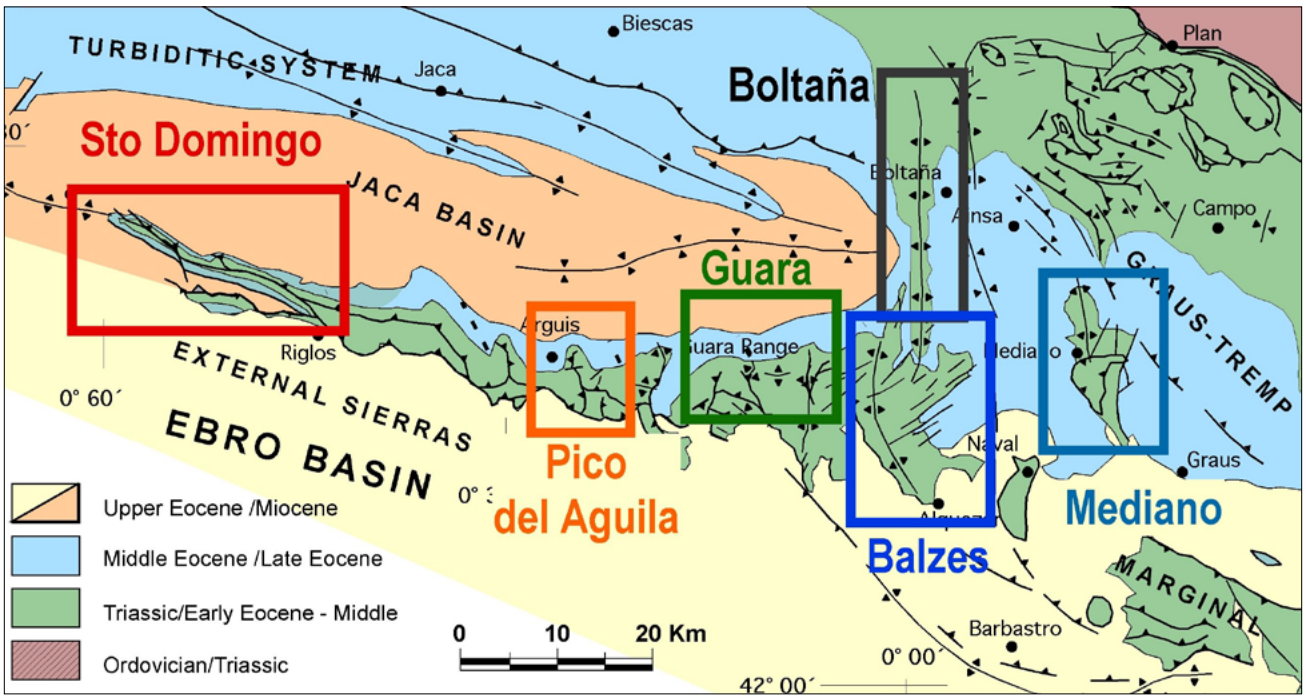

FIGURE 15. Location of structures with available rotational kinematic data in the Southwestern Pyrenees.

TABLE 4. Mean paleomagnetic vectors derived from the age-grouping of paleomagnetic sites in the northern sector of the Balzes anticline. S: number of sites considered in the grouping, see Table 2 caption for the other abbreviations

Group	Age-mean	Age-StaDev	S	Dec-ABC	Inc-ABC	α95	*k*	R	Thrust sheet
A	45.13	0.57	4	68.7	34.1	5.2	318.3	0.9976	Balzes thrust sheet
B	43.04	0.79	5	49.6	41.2	9.6	63.9	0.9875	Balzes thrust sheet
C	41.61	0.28	5	45.6	38.0	22.7	12.3	0.9348	Balzes thrust sheet
D	40.31	0.45	5	34.0	39.0	18.5	18.0	0.9556	Balzes thrust sheet
E	38.77	0.81	5	10.9	37.4	12.8	36.6	0.9781	Balzes thrust sheet
F	38.36	1.68	4	30.5	29.0	7.0	30.1	0.9751	Guara thrust sheet
G	34.90	1.74	7	1.4	39.7	11.9	42.2	0.9811	Guara thrust sheet

paleomagnetic study of the westernmost Santo Domingo anticline along the Salinas magnetostratigraphic section (Hogan, 1993). We have plotted together all the available data, although with different degrees of completion in Figure 16. This graph synthetizes 20Ma of rotational activity related to the South Pyrenean front evolution from Ypresian to Rupelian times and allows highlighting some key observations:

- Comparable rotation velocities occur in those structures that are well characterized, specially during the main rotational periods that range between 7º to 12º/Ma.

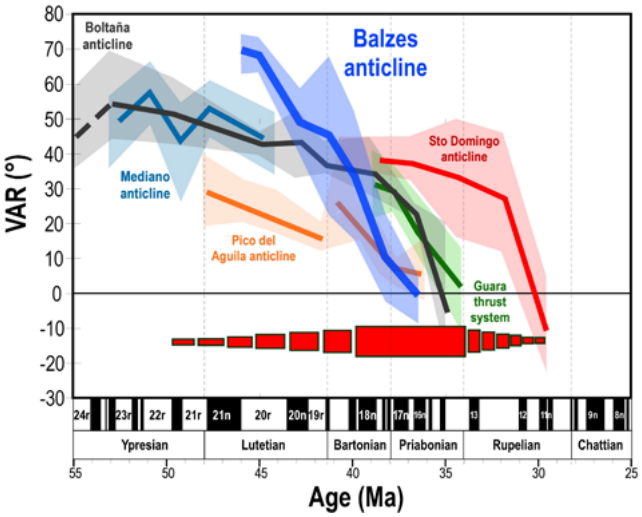

FIGURE 16. Rotation velocity and timing of some oblique South Pyrenean structures. Light blue line: data from the Mediano anticline (Muñoz *et al.*, 2013; Beamud *et al.*, 2017). Orange line: data from Pico del Águila (Pueyo *et al.*, 2002; Rodriguez-Pintó *et al.*, 2008). Green line: data from the northern sector of the Guara thrust system (Pueyo, 2000; Pueyo *et al.*, 2003b). Dark blue line: data from the Balzes anticline (Rodriguez-Pintó *et al.*, 2016, 2020 and this work). Black line: data from the Boltaña anticline (Mochales *et al.*, 2012a). Red line: data from the Santo Domingo anticline (Pueyo *et al.*, 2021). The light area around the data corresponds to the α95 angle of the related fisherian means. Thrusting kinematics of the Gavarnie thrust sheet (Oliva-Urcia, 2018 and references therein) is also shown as red rectangles.

- More moderate paces (1º-3º/Ma) are noticed for those structures showing two distinct rotational periods (Pico del Aguila, Boltaña and Santo Domingo).

- The main rotational activity coincides with Bartonian-Priabonian times, except for the Santo Domingo anticline, at the western corner of the External Sierras front, which displays a significant younger age (main rotational activity during Upper Rupelian times, more than 5Ma later)

The last observation strengthens the diachronic character of the along-strike rotational movements of the South Pyrenean sole thrust. Besides, the end of the rotational activity of the thrust sheets vanishes along-strike at a pace of 9km/Ma, considering the distance between the Balzes and Santo Domingo anticlines. Regarding the onset of rotation, similar ages may be expected if the lateral migration pattern of the deformation front in the External Sierras (5m/ma) is taken into account (Millán *et al.*, 2000). In any case, the regional moderate rotation related to the Guarga activity (Muñoz *et al.*, 2013) is more complex and it is likely compartmented in other intermediate and older basement thrust sheets (*e.g.* Fiscal-Broto). Further data (Beamud *et al.*, in progress) in the Eastern end-member Mediano anticline) may shed light on the problem and will help understanding the 4D architecture of the South Pyrenean thrust system.

CONCLUSIONS

The new 950m magnetostratigraphic section (Las Bellostas) across Cuisian-Lutetian and Bartonian times introduced in this paper is characterized by primary magnetization, that allows building a reliable LPS with 8 magnetozones that can be correlated to the GPTS with the support of biostratigraphic data from seven new studied levels. This new data allows reaching the following conclusions:

i) A sedimentary hiatus is found between Cuisian (late Ypresian) and Lutetian times, specifically between chrons C22n to C20n. This unconformity, which was described previously by Barnolas and Gil-Peña (2001), Rodríguez-Pintó *et al.* (2016) and Barnolas *et al.* (2019) is younger tan the observed in the San Pelegrín and at the base of the Isuela sections (Rodríguez-Pintó *et al.*, 2012a, 2013a respectively).

ii) The onset of the continental sedimentation in the southeasternmost sector of the Jaca Basin can be dated in C18r, at the base of the Bartonian, and is coeval with the deltaic facies of the Belsué-Atarés Fm. to the west of the Gabardiella anticline and with the prodeltaic marls of the Arguis Fm. to the west of the Pico del Aguila anticline.

iii) The close genetic relationship between the Escanilla and Campodarbe fms. is reinforced with the chronostratigraphic data from Las Bellostas section presented here, and with the recently published data from the Olsón section (Vinyoles *et al.*, 2020). This allows for an accurate correlation between both formations. The stratigraphic sequence of the Campodarbe Fm. in the Las Bellostas section reflects an increase of in clasts from Mesozoic and Cenozoic source rocks during the early Bartonian (subunits 2 to 4). A shift from clasts of Variscan sources to Mesozoic-Cenozoic clasts in conglomerates, paired with N-S paleocurrents, was pointed out previously in the Escanilla Fm. (Olsón Mbr.) by Dreyer *et al.* (1993) near the C18r/C18n boundary (Bentham *et al.*, 1992).

The age of Las Bellostas section is also coeval to the rotational movement of the underneath Balzes-Boltaña thrust sheet (part of the imbricate system of the South Pyrenean sole thrust) and thus, records with accuracy the rotational kinematics:

IV) The rotational movement onset can be dated, at least, during Lutetian times (chron C20r) synchronously to the folding of the Balzes anticline. The rotation activity totally vanishes in Middle Priabonian (C17-C16). The total accumulated rotation magnitude recorded in the Lutetian exceeds 70ºCW.

V) The rotation velocity during this period fits very well with constant rate around 9-11º/Ma, (regressions coefficients between 0.8331 and 0.9587).

This rotational kinematics is coeval to closer structures (Boltaña, Pico del Aguila and Guara system) but substantially differs from distant ones (Santo Domingo anticline to the west). The linear and continuous pattern of rotation found in the Balzes-Boltaña thrust sheet differs from most South Pyrenean structures, which usually display two distinct rotational periods.

ACKNOWLEDGMENTS

This paper represents our modest tribute to Pep Serra-Kiel for his inspiring work, his sharp intelligence, his working tenacity, his always fruitful discussions and his camaraderie and friendship. This work was financed by the Sobrarbe County Research fellow-UNESCO Global Geopark (ARP) and by some projects from the Spanish Science National Plan (UKRIA4D- PID2019-104693GB-I00/CTA, DR3AM. CGL2014 54118-C2-2-R and MAGIBER-II. CGL2017-90632-REDT). We are also very grateful to the laboratories of the universities of Burgos (Juanjo Villalaín) and Zaragoza (Teresa Román and Sylvia Gracia), Sergio Arruej Gil for the field support and Pablo Calvin and Vicky Burriel for the Burgos logistic support. Very warm acknowledged is given to Alejandro and Pablo from "Casa Molinero" in Las Bellostas for their hospitality, friendship and human warmth during all these years. Finally, we sincerely acknowledge the thorough and constructive reviews done by Miguel Garcés, Josep Tosquella and the editor Carles Martín-Closas.

REFERENCES

Allmendinger, R.W., Cardozo, N.C., Fisher, D., 2013. Structural geology algorithms: Vectors & tensors. Cambridge, Cambridge University Press, 289pp.

Anastasio, D.J., Holl, J.E., 2001. Transverse fold evolution in the External Sierra, southern Pyrenees, Spain. Journal of Structural Geology, 23, 379-392.

Anastasio, D.J., Teletzke, A.L., Kodama, K.P., Parés, J.M., Gunderson, K.L., 2020. Geologic evolution of the Peña flexure, Southwestern Pyrenees mountain front, Spain. Journal of Structural Geology,131, 103969.

Arenas, C., Millán, H., Pardo, G., Pocoví, A., 2001. Ebro Basin continental sedimentation associated with late compressional Pyrenean tectonics (north-eastern Iberia): controls on basin margin fans and fluvial systems. Basin Research, 13(1), 65-89.

Barnolas, A., Gil-Peña, I., 2001. Ejemplos de relleno sedimentario multiepisódico en una cuenca de antepaís fragmentada: La

Cuenca Surpirenaica. Boletín Geológico y Minero, 112(3), 17-38.

Barnolas, A., Larrasoaña, J.C., Pujalte, V., Schmitz, B., Sierro, F.J., Mata, M.P., .. van den Berg, .C.J., Pérez-Asensio, J.N., Salazar, A., Salvany, J.M., Ledesma, S., García-Castellanos, D., Civis, J., Cunha, P.P. 2019. Alpine foreland basins. In: The Geology of Iberia: A Geodynamic Approach. C. Quesada and J. T. Oliveira (eds.). Cham, Springer, 7-59.

Beamud, E., Pueyo, E.L., Muñoz, J.A., Valero, L., Granado, P., 2017. Paleomagnetic constraints on the kinematics of the Mediano Anticline (Aínsa Basin). Preliminary results. MAGIBER X. Instituto Universitario de Ciencias Amientales IUCA-University of Zaragoza. ISBN: 978-84-16723-40-9, 34-37.

Bentham, P., Burbank, D.W., 1996. Chronology of Eocene foreland basin evolution along the western oblique margin of the South-Central Pyrenees. In: Friend, P.F., Dabrio, C.J. (eds.). Tertiary basind of Spain. Cambridgem Cambridge University Press, 144-152.

Burbank, D.W., Raynolds, R.G., 1988. Stratigraphic keys to the timing of thrusting in terrestrial foreland basins: Applications to the northwestern Himalaya. In: Kleinspehn, K.L., Paola, C. (eds) New Perspectives in Basin Analysis. Frontiers in Sedimentary Geology. Springer, New York, 331-351.

Burbank, D.W., Vergés, J., Muñoz, J.A., Bentham, P., 1992. Coeval hindward-and forward-imbricating thrusting in the south-central Pyrenees, Spain: Timing and rates of shortening and deposition. Geological Society of America Bulletin, 104(1), 3-17.

Calvín, P., Villalaín, J.J., Casas-Sainz, A.M., Tauxe, L., Torres-López, S., 2017. pySCu: A new Python code for analyzing remagnetizations directions by means of small circle utilities. Computers & Geosciences, 109, 32-42.

Calvín, P., Pueyo, E.L., Ramón, M.J., Casas-Sainz, A.M., Villalaín, J.J., 2020. Analysing non-coaxial folding effects in the Small Circle Intersection method. Geophysical Journal International, 222(2),940-955.

Canudo, J.I., Molina, E., 1992. Bioestratigrafía con foraminíferos planctónicos del Paleógeno del Pirineo. Neues Jahrbuch fur Geologie und Palaontologie - Abhandlungen, 186(1-2), 97-135. DOI: 10.1144/jgs2020-085

Canudo, J.I., Molina, E., Riveline, J., Serra-Kiel, J., Sucunza, M., 1988. Évènements biostratigraphiques pendant l'Éocène Moyen-Oligocéne inférieur dans les Prépyrénées d'Aragon (Espagne). Revue de Micropaléontologie, 31, 15-29.

Casas, A.M., Pardo, G., 2004. Estructura pirenaica y evolución de las cuencas sedimentarias en la transversal Huesca-Oloron. In: Colombo, F., Liesa, C.L., Meléndez, G., Pocovi, A., Sancho, C., Soria, A.R. (eds.). Itinerarios geológicos por Aragón. Sociedad Geológica de España, Geo Guías, 1, 63-96. ISBN: 84-930160-2-0.

Chen, J., Burbank, D.W., Scharer, K.M., Sobel, E., Yin, J., Rubin, C., Zhao, R., 2002. Magnetochronology of the Upper Cenozoic strata in the Southwestern Chinese Tian Shan: rates of Pleistocene folding and thrusting. Earth and Planetary Science Letters, 195(1-2), 113-130.

Costa, E., Garcés, M., López-Blanco, M., Beamud, E., Gómez-Paccard, M., Larrasoaña, J.C., 2010. Closing and continentalization of the South Pyrenean foreland basin (NE Spain): magnetochronological constraints. Basin Research, 22(6), 904-917.

Cox, A., Doell, R.R., Dalrymple, G.B., 1963. Geomagnetic polarity epochs and Pleistocene geochronometry. Nature, 198(4885), 1049-1051.

Deenen, M.H.L., Langereis, C.G., van Hinsbergen, D.J.J., Biggin, A.J., 2011. Geomagnetic secular variation and the statistics of palaeomagnetic directions. Geophysical Journal International, 186(2), 509-520.

De Federico, A., 1981. La sedimentación de talud en el sector occidental de la cuenca paleógena de Ainsa. Ph.D. Thesis. Bellaterra, Autonomous University of Barcelona. Publicaciones e Geología 12, 281 pp..

Dreyer, T., Fält, L.M., Høy, T., Knarud, R., Steel, R., Cuevas, J.-L., 1993. Sedimentary architecture of field analogues for reservoir information (SAFARI): a case study of the fluvial Escanilla Formation, Spanish Pyrenees. In: Flint, S., Bryant, I.D. (eds.). The Geological Modelling of Hydrocarbon Reservoirs and Outcrop Analogues. International Association of Sedimentologists Special Publications 15, 57-80.

Dreyer, T., Corregidor, J., Arbues, P., Puigdefàbregas, C., 1999. Architecture of the tectonically influenced Sobrarbe deltaic complex in the Ainsa Basin, northern Spain. Sedimentary Geology, 127, 127-169.

Fisher, R.A., 1953. Dispersion on a sphere. Proceedings of the Royal Society of London. Series A. Mathematical and Physical Sciences, 217(1130), 295-305.

Garcés, M., López-Blanco, M., Valero, L., Beamud, E., Pueyo, E.L., Rodríguez-Pintó, A., 2014. Testing orbital forcing in the Eocene deltaic sequences of the South-Pyrenean Foreland Basins. Geophysical Research Abstracts, 16, EGU2014-10681-1.

Garcés, M., López-Blanco, M., Valero, L., Beamud, E., Muñoz, J.A., Oliva-Urcia, B., Vinyoles, A., Arbués, P., Cabello, P. Cabrera, L., 2020. Paleogeographic and sedimentary evolution of the South Pyrenean foreland basin. Marine and Petroleum Geology, 113, 104105.

Heller, P.L., Paola, C., 1992. The large-scale dynamics of grain-size variation in alluvial basins, 2: Application to syntectonic conglomerate. Basin Research, 4(2), 91-102.

Hogan, P.J., 1993. Geocrohonologic, tectonic and stratigraphic evolution of the Southwest Pyrenean foreland basin, Northern Spain. PhD Thesis. University of Southern California, Los Angeles unpublised, 219pp.

Hogan, P.J., Burbank, D.W., 1996. Evolution of the Jaca piggyback basin and emergence of the External Sierra, southern Pyrenees. In: Friend, P.F., Dabrio, C.J. (eds.). Tertiary basins of Spain. Cambridge, Cambridge University Press, 153-160.

Izquierdo-Llavall, E., Sainz, A.C., Oliva-Urcia, B., Burmester, R., Pueyo, E.L., Housen, B., 2015. Multiepisodic remagnetization related to deformation in the Pyrenean Internal Sierras. Geophysical Journal International, 201(2), 891-914.

Johnson, N.M., McGee, V.E., 1983. Magnetic polarity stratigraphy: Stochastic properties of data, sampling problems, and the evaluation of interpretations. Journal of Geophysical Research: Solid Earth, 88(B2), 1213-1221.

Kirschvink, J.L., 1980. The least-squares line and plane and the analysis of palaeomagnetic data. Geophysical Journal International, 62(3), 699-718.

Kjemperud, A.V., Schomacker, E., Brendsdal, A., Fält, L.-M., Jahren, J.S., Nystuen, J.P., Puigdefàbregas, C., 2004. The Fluvial Analogue Escanilla Formation, Ainsa Basin, Spanish Pyrenees: Revisited. American Asociation of Petroleoum Geologist Search and Discovery, Article #30026, 8pp.

Kodama, K.P., Anastasio, D.J., Newton, M.L., Pares, J.M., Hinnov, L.A., 2010. High resolution rock magnetic cyclostratigraphy in an Eocene flysch, Spanish Pyrenees. Geochemistry, Geophysics, Geosystems, 11, Q0AA07-22 pages.

Labaume, P., Teixell, A., 2018. 3D structure of subsurface thrusts in the eastern Jaca Basin, southern Pyrenees. Geologica Acta, 16(4), 477-498.

Labaume, P., Séguret, M., Seyve, C., 1985. Evolution of a turbiditic foreland basin and analogy with an accretionary prism: Example of the Eocene south□Pyrenean basin. Tectonics, 4(7), 661-685.

Labaume, P., Meresse, F., Jolivet, M., Teixell, A., Lahfid, A., 2016. Tectonothermal history of an exhumed thrust□sheet□top basin: An example from the south Pyrenean thrust belt. Tectonics, 35(5), 1280-1313.

Larrasoaña, J.C., Parés, J.C., Pueyo, E.L., 2003. Stable Eocene magnetization carried by magnetite and magnetic iron sulphides in marine marls (Pamplona-Arguis Formation, southern Pyrenees, N Spain). Studia Geophysica Geodetica, 47, 237-254.

Larrasoaña, J.C., Pueyo, E.L., Parés, J.M., 2004. An integrated AMS, structural, palaeo-and rock magnetic study of Eocene marine marls from the Jaca-Pamplona basin (Pyrenees, N Spain); new insights into the timing of magnetic fabric acquisition in weakly deformed mudrocks. London, The Geological Society, 238(1, Special Publications), 127-143.

Lowrie, W., 1990. Identification of ferromagnetic minerals in a rock by coercivity and unblocking temperature properties. Geophysical research letters, 17(2), 159-162.

Luzón, A., 2005. Oligocene–Miocene alluvial sedimentation in the northern Ebro Basin, NE Spain: Tectonic control and palaeogeographical evolution. Sedimentary Geology, 177(1-2), 19-39.

Mateu-Vicens, G., Pomar, L., Ferrandez-Cañadell, C., 2012. Nummulitic banks in the upper Lutetian "Buil level", Ainsa basin, South Central pyrenean zone: the impact of internal waves. Sedimentology, 59, 527-552.

McElroy, R., 1990. Thrust kinematics and syntectonic sedimentation: the Pyrenean frontal ramp, Huesca, Spain. PhD Thesis. Cambridge, University of Cambridge, unpublished, 175pp.

McFadden, P.L., 1990. A new fold test for palaeomagnetic studies. Geophysical Journal International, 103(1), 163-169.

Meresse, F., 2010. Dynamique d'un prisme orogénique intracontinental: évolution thermochronologique (traces de fission sur apatite) et tectonique de la Zone Axiale et des piémonts des Pyrénées centro-occidentales. Doctoral Dissertation. Montpellier, Université de Montpellier 2, 280pp.

Millán, H., 1996. Estructura y cinemática del frente de cabalgamiento surpirenaico en las Sierras Exteriores Aragonesas. Tesis Doctoral Zaragoza. Universidad de Zaragoza, 330pp.

Millán, H., Pueyo, E.L., Aurell, M., Luzón, A., Oliva-Urcia, B., Martínez Peña, M.B., Pocoví, A., 2000. Actividad tectónica registrada en los depósitos terciarios del frente meridional del Pirineo central. Revista de la Sociedad Geológica de España, 13(2), 117-138.

Millán Garrido, H., Oliva-Urcia, B., Pocoví-Juan, A., 2006. La transversal de Gavarnie-Guara; estructura y edad de los mantos de Gavarnie, Guara-Gedre y Guarga (Pirineo centro-occidental). Geogaceta, 40, 35-38.

Mochales, T., Casas, A.M., Pueyo, E.L., Barnolas, A., 2012a. Rotational velocity for oblique structures (Boltaña anticline, Southern Pyrenees). Journal of Structural Geology, 35, 2-16.

Mochales, T., Barnolas, A., Pueyo, E.L., Serra-Kiel, J., Casas, A.M., Samsó, J.M., Ramajo, J., Sanjuán, J., 2012b. Chronostratigraphy of the Boltaña anticline and the Ainsa Basin (southern Pyrenees). Geological Society of America Bulletin, 124(7-8), 1229-1250.

Mochales, T., Pueyo, E.L., Casas, A.M., Barnolas, A., 2016. Restoring paleomagnetic data in complex superposed folding settings: The Boltaña anticline (Southern Pyrenees). Tectonophysics, 671, 281-298.

Molina, E., Alegret, L., Serra-Kiel, J., 2013. Los microfósiles del Prepirineo de Arguis (Huesca): breve guía para observarlos y reconocerlos. Naturaleza Aragonesa, 30, 4-12. ISSN: 1138-8013

Montes-Santiago, M.J., 1992. Sistemas deposicionales en el Eoceno medio-Oligoceno del sinclinorio del Guarga (Cuenca de Jaca, Pirineo central). Salamanca, Simposio sobre Geología de los Pirineos, III Congreso Geológico de España, 2, 150-160.

Montes-Santiago, M.J., 2002. Estratigrafía del Eoceno-Oligoceno de la cuenca de Jaca (sinclinorio del Guarga). PhD Dissertation. Barcelona, Universitat de Barcelona, 365 pages.

Montes-Santiago, M.J., 2009. Estratigrafía del Eoceno-Oligoceno de la cuenca de Jaca (sinclinorio del Guarga). Instituto de Estudios Altoaragoneses, Colección de estudios altoaragoneses, 59, 355pp. ISBN: 8481272027.

Muñoz, J.A., 1992. Evolution of a continental collision belt: ECORS-Pyrenees crustal balanced cross section. In: McClay, K.R. (ed.). Thrust tectonics. Dordrecht, Springer, 235-246.

Muñoz, J.A., 2019. Alpine Orogeny: Deformation and Structure in the Northern Iberian Margin (Pyrenees sl). In: The Geology of Iberia: A Geodynamic Approach. C. Quesada and J. T. Oliveira (eds.) Cham, Springer, 433-451.

Muñoz, J.A., Beamud, E., Fernández, O., Arbués, P., Dinarès-Turell, J., Poblet, J., 2013. The Aínsa Fold and thrust oblique zone of

the central Pyrenees: Kinematics of a curved contractional system from paleomagnetic and structural data. Tectonics, 32(5), 1142-1175.

Norris, D.K., Black, R.F, 1961. Application of palaeomagnetism to thrust mechanics. Nature, 192(4806), 933-935.

Ogg, J.G., 2012. Geomagnetic Polarity Time Scale. In: Gradstein, F.M., Ogg, J.G., Schmitz, M., Ogg, G. (eds.). The Geologic Time Scale. Oxford, Elsevier, 85-113.

Oliva-Urcia, B., 2018. Thirty years (1988-2018) of advances in the knowledge of the structural evolution of the South-Central Pyrenees during the Cenozoic collision, a summary. Revista de la Sociedad Geológica de España, 31(2), 51-68.

Oliva-Urcia, B., Pueyo, E.L., 2007. Rotational basement kinematics deduced from remagnetized cover rocks (Internal Sierras, southwestern Pyrenees). Tectonics, 26(4), TC4014, 22 pages.

Oliva-Urcia, B., Pueyo E.L., 2019 Paleomagnetism in structural geology and tectonics. In: Mukherjee, S. (ed.). Teaching methodologies in structural geology and tectonics. Heidelberg, Springer, 55-121. ISBN: 978-981-13-2781-0. 1.

Oliva-Urcia, B., Beamud, E., Garcés, M., Arenas, C., Soto, R., Pueyo, E.L., Pardo, G., 2016. New magnetostratigraphic dating of the Palaeogene syntectonic sediments of the west-central Pyrenees: tectonostratigraphic implications. London, The Geological Society, 425 (Special Publications), SP425-5.

Oliva-Urcia, B., Beamud, E., Arenas, C., Pueyo, E.L., Garcés, M., Soto, R., Valero, L., Pérez-Rivarés, F.J., 2019. Dating the northern deposits of the Ebro foreland basin; implications for the kinematics of the SW Pyrenean front. Tectonophysics, 765, 11-34.

Oms, O., Dinarès-Turell, J., Remacha, E., 2003. Magnetic stratigraphy from deep clastic turbidites: an example from the Eocene Hecho group (southern Pyrenees). Studia Geophysica et Geodaetica, 47(2), 275-288.

Opdyke, M.D., Channell, J.E., 1996. Magnetic stratigraphy. Academic press, 64, 346pp.

Pérez-Rivarés, F.J., Arenas, C., Pardo, G., Garcés, M., 2018. Temporal aspects of genetic stratigraphic units in continental sedimentary basins: Examples from the Ebro basin, Spain. Earth-Science Reviews, 178, 136-153.

Pocoví, A., 2019. Geología pirenaica vista desde el Sur. Real Academia de Ciencias Exactas, Físicas, Químicas y Naturales de Zaragoza, Discurso de Ingreso, Depósito legal: Z 592-2019: Servicio de Publicaciones, Universidad de Zaragoza, 122pp.

Pueyo-Anchuela, Ó., Pueyo, E.L., Pocoví-Juan, A., Gil-Imaz, A., 2012. Vertical axis rotations in fold and thrust belts: comparison of AMS and paleomagnetic data in the Western External Sierras (Southern Pyrenees). Tectonophysics, 532, 119-133.

Pueyo, E.L., 2000. Rotaciones paleomagnéticas en sistemas de pliegues y cabalgamientos. Tipos, causas, significado y aplicaciones (ejemplos del Pirineo Aragonés). PhD Thesis Zaragoza. Universidad de Zaragoza, Unpublished, 296pp.

Pueyo, E.L., Millán, H., Pocoví, A., Parés, J.M., 1997. Cinemática rotacional del cabalgamiento basal surpirenaico en las Sierras Exteriores Aragonesas: Datos magnetotectónicos. Acta geológica hispánica, 32(3), 237-256.

Pueyo, E.L., Millán, H., Pocoví, A., 2002. Rotation velocity of a thrust: a paleomagnetic study in the External Sierras (Southern Pyrenees). In: Marzo, M., Muñoz, J.A., Vergés, J. (eds.). Growth strata. Sedimentary Geology, 146, 191-208. DOI: 10.1016/S0037-0738(01)00172-5

Pueyo, E.L., Pocoví, A., Parés, J.M., Millán, H., Larrasoaña, J.C., 2003. Thrust ramp geometry and spurious rotations of paleomagnetic vectors. Studia Geophysica et Geodaetica, 47(2), 331-357.

Pueyo, E.L., Oliva-Urcia, B., Sussman, A.J., Cifelli, F., 2016. Palaeomagnetism in Fold and Thrust Belts: Use with caution. In: Pueyo, E.L., Cifelli, F., Sussman, A., Oliva-Urcia, B. (eds.). Palaeomagnetism in Fold and Thrust Belts: New Perspectives. London, The Geological Society, 425(1, Special Publications), 259-276.

Pueyo, E.L., García-Lasanta, C., López, M.A., Oliván, C., Miguel, G.S., Gil-Garbi, H., Oliva-Urcia, B., Beamud, E., Hernández, R., Elger, K., Ulbricht, D., Lange, O., the GeoKin3DPyr group, 2017. Metodología para el desarrollo de la BBDD paleomagnética de Iberia (EPOS-DDSS Iberian Paleomagnetism). MAGIBER X., IUCA- Universidad de Zaragoza, 94-99.

Pueyo, E.L., Oliva-Urcia, B., Sánchez-Moreno, E.M., Arenas, C., Silva-Casal, R., Calvín, P., Santolaria, P., García-Lasanta, C., Oliván, C., Compaired, F., Casas, A.M., Pocoví, A., 2021. The Geometry and Kinematics of the Southwestern Termination of the Pyrenees: A Field Guide to the Santo Domingo Anticline. In: Soumyajit Mukherjee (ed.). Structural Geology and Tectonics Field Guidebook. Singapore, Springer, 1(3), 49-101.

Puigdefábregas, C., 1975. La sedimentación molásica en la cuenca de Jaca. Pirineos, 104, 1-188.

Pujalte, V., Baceta, J.I., Schmitz, B., Orue-Etxebarria, X., Payros, A., Bernaola, G., Apellaniz, E., Caballero, F., Robador, A., Serra-Kiel, J., Tosquella, J., 2009. Redefinition of the Ilerdian Stage (early Eocene). Geologica Acta, 7(1-2), 177-194.

Ramón, M.J., Pueyo E.L., Oliva-Urcia, B., Larrasoaña, J.C., 2017. Virtual directions in paleomagnetism: A global and rapid approach to evaluate the NRM components and their stability. Frontiers in Earth Science, 5(8), 14pp.

Riba, O., 1976. Syntectonic unconformities of the Alto Cardener, Spanish Pyrenees: a genetic interpretation. Sedimentary Geology, 15(3), 213-233.

Rodríguez-Pintó, A., 2013. Magnetoestratigrafía del Eoceno inferior y medio en el frente Surpirenaico (Sierras Exteriores): implicaciones cronoestratigráficas y cinemáticas. PhD Thesis. University of Zaragoza, Unpublished, 370pp. Last accessed:August 2022. Website: http://zaguan.unizar.es/record/10043

Rodríguez-Pintó, A., Pueyo, E.L., Pocoví, A., Barnolas, A., 2008. Cronología de la actividad rotacional en el sector central del frente de cabalgamiento de Sierras Exteriores (Pirineo Occidental). Geotemas, 10, 1207-1210.

Rodríguez-Pintó, A., Pueyo, E.L., Serra-Kiel, J., Samsó, J.M., Barnolas, A., Pocoví, A., 2012a. Lutetian magnetostratigraphic calibration of larger foraminifera zonation (SBZ) in the Southern Pyrenees: The Isuela section. Palaeogeography, Palaeoclimatology, Palaeoecology, 333-334, 107-120.

Rodríguez-Pintó, A., Pueyo, E.L., Barnolas, A., Samsó, J.M., Pocoví, A., Gil-Peña, I., Mochales, T., Serra-Kiel, J., 2012b. Lutetian magnetostratigraphy in the Santa Marina section (Balzes anticline, Southwestern Pyrenees). Geotemas, 13, 1184-1187.

Rodríguez-Pintó, A., Pueyo, E.L., Serra-Kiel, J., Barnolas, A., Samsó, J.M., Pocoví, A., 2013a. The Upper Ypresian-Lutetian in the San Pelegrín section (Southwestern Pyrenean Basin): magnetostratigraphy and larger foraminifera correlation. Palaeogeography, Palaeoclimatology, Palaeoecology 370, 13-29.

Rodríguez-Pintó, A., Pueyo, E.L., Barnolas, A., Pocoví, A., Oliva-Urcia, B., Ramón, M.J., 2013b. Overlapped paleomagnetic vectors and fold geometry: a case study in the Balzes anticline (Southern Pyrenees). Physics of the Earth and Planetary Interiors, 215, 43-57.

Rodríguez-Pintó, A., Pueyo, E.L., Sánchez, E., Calvin, P., Ramajo, J., Ramón, M.J., Pocoví, A., Barnolas, A., Casas, A.M., 2016. Rotational kinematics of a curved fold: a structural and paleomagnetic study in the Balzes anticline (Southern Pyrenees). Tectonophysics, 677-678, 171-189.

Rodríguez-Pintó, A., Sanchez, E., Barnolas, A., Serra-Kiel, J., Samsó, J.M., Mochales, T., Pueyo, E.L., Scholger, R., 2017. Magnetostratigraphic data from lower part of Gabardiella section: Early Middle Eocene, Southern Pyrenees. MAGIBER X Valle del Grío, Universidad de Zaragoza, 30-33pp. ISBN: 978-84-16723-40-9.

Rodríguez-Pintó, A., Sánchez-Moreno, E., Pueyo, E.L., Oliva-Urcia, B., Barnolas, A., Izquierdo-Llavall, E., 2019. Limite Luteciense/Bartoniense en la sección de Isuela (revisada), Pirineos suroccidentales. In: Font, E., Beamud, E., Oliva-Urcia, B., Pueyo, E.L., Lopez, F.C. Livro de Resumos. MAGIBER XI PALEOMAGNETISMO EN ESPANHA E PORTUGAL. Universidade de Coimbra, 121-124. ISBN 978-989-98914-7-0.

Rodríguez-Pintó, A., Pueyo, E.L., Sánchez-Moreno, E.M., 2020. Paleomagnetic data of the Balzes Anticline. Deutsches GeoForschungs Zentrum GFZ Data Services. DOI: https://doi.org/10.5880/fidgeo.2020.041

Sagnotti, L., Roberts, A.P., Weaver, R., Verosub, K.L., Florindo, F., Pike, C.R., Wilson, G.S., 2005. Apparent magnetic polarity reversals due to remagnetization resulting from late diagenetic growth of greigite from siderite. Geophysical Journal International, 160(1), 89-100.

Samsó, J.M., Serra-Kiel, J., Tosquella, J., Travé, A., 1994. Cronoestratigrafía de las plataformas lutecienses de la zona central de la cuenca surpirenaica. Jaca, II Congreso del Grupo Español del Terciario, Comunicaciones, 205-208.

Santolaria, P., Ayala, C., Pueyo, E.L., Rubio, F.M., Soto, R., Calvín, P., Casas-Sainz, A.M., 2020. Structural and geophysical characterization of the western termination of the South Pyrenean triangle zone. Tectonics, 39(8), e2019TC005891.

Schaub, H., 1981. Nummulites et Assilines de la Tethys paléogène. Taxinomie, phylogénèse et biostratigraphie. Mémoires suisses de Paléontologie, 104, 1-236 and 105-106, 97pls.

Schaub, H., 1992. The Campo section (NE Spain), a Tethyan parastratotype of the Cuisian. Abhandlungen, Neues Jahrbuch für Geologie und Paläontologie, 186, 63-70.

Serra-Kiel, J., Hottinger, L., Caus, E., Drobne, K., Ferràndez, C., Jauhri, A.K., Less, G., Pavlovec, R., Pignatti, J., Samsó, J.M., Schaub, H., Sirel, E., Strougo, A., Tambareau, Y., Tosquella, J., Zakrevskaya, E., 1998. Larger foraminiferal biostratigraphy of the Tethyan Paleocene and Eocene. Bulletin de la Société Géologique de France, 169(2), 281-299.

Serra-Kiel, J., Travé, A., Mató, E., Saula, E., Ferrández-Cañadell, C., Busquets, P., Tosquella, J., Vergés, J., 2003. Marine and Transitional Middle/Upper Eocene Units of the Southeastern Pyrenean Foreland Basin (NE Spain). Geologica Acta (Acta Geologica Hispanica), 1(2), 177-200.

Serra-Kiel, J., Vicedo, V., Baceta, J.I., Bernaola, G., Robador, A., 2020. Paleocene Larger Foraminifera from the Pyrenean Basin with a recalibration of the Paleocene Shallow Benthic Zones. Geologica Acta, 18(8), 1-69, I-III.

Silva-Casal, R., Aurell, M., Payros, A., Pueyo, E.L., Serra-Kiel, J., 2019. Carbonate ramp drowning caused by flexural subsidence: The South Pyrenean middle Eocene foreland basin. Sedimentary Geology, 393-394, 105538, 23pp.

Silva-Casal, R., Serra-Kiel, J., Rodríguez-Pintó, A., Pueyo, E.L., Aurell, M., Payros, A., 2021 Systematics of Lutetian Larger Foraminifera and magneto-biostratigraphy from the South Pyrenean Basin (Sierras Exteriores, Spain). Geologica Acta, 19, 1-64, I-XVII.

Soler, M., Puigdefàbregas, C., 1970. Líneas generals de la geología del Alto Aragón occidental. Pirineos, 96, 5-20.

Sussman, A.J., Weil, A.B., 2004. Orogenic curvature: Integrating paleomagnetic and structural analyses Geological Society of America, 383 (Special Paper), 271 pp.

Talling, P.J., Burbank, D.W., 1993. Assessment of uncertainties in magnetostratigraphic dating of sedimentary strata. In: Aissaoui DM, McNeill DF, Hurley NF (eds) Applications of paleomagnetism to sedimentary geology. Society for Sedimentary Geology (SEMP) special publication, 49, 59-69.

Tauxe, L., Gallet, Y., 1991. A jackknife for magnetostratigraphy. Geophysical Research Letters, 18(9), 1783-1786.

Toro, R., Casas, A.M., Izquierdo-Llavall, E., Pueyo, E.L., Navas, J., Peropadre, C., Martín, J., 2021. 3D basement geometry of the southwestern Pyrenees from seismic exploration. X Congreso Geológico de España, Geotemas, 18, 565.

Vandamme, D., 1994. A new method to determine paleosecular variation. Physics of the Earth and Planetary Interiors, 85(1-2), 131-142.

Valero, L., Vinyoles, A., Garcés, M., López-Blanco, M., Beamud, E., Pueyo-Morer, E., Rodríguez-Pintó, A., Sharma, N.,

Watkins, S., Castelltort, S., 2020. Orbital origin of the stratigraphic sequences in South-Pyrenean syn-kinematic sediments. Zurich, 18th Swiss Geoscience Meeting, 2020-08-21-20-04-44-27

Vinyoles, A., 2021. Sediment routing systems of the Eocene Tremp-Jaca basin: Stratigraphic analysis and numerical models. PhD Thesis. Barcelona, Universitat de Barcelona, unpublished, 146pp.

Vinyoles, A., López-Blanco, M., Garcés, M., Arbués, P., Valero, L., Beamud, E., Oliva-Urcia, B., Cabello, P., 2020. 10 Myr evolution of sedimentation rates in a deep marine-nonmarine foreland basin system: tectonic and sedimentary controls (Eocene, Tremp-Jaca Basin, Southern Pyrenees, NE Spain). Basin Research, 33(1), 447-477.

Waldhör, M., Appel, E., 2006. Intersections of remanence small circles: new tools to improve data processing and interpretation in palaeomagnetism. Geophysical Journal International, 166(1), 33-45.

Zijderveld, J.D.A., 1967. AC Demagnetization of Rocks: Analysis of Results. In: Runcorn, S.K., Creer, K.M., Collinson, D.W. (eds.). Methods in Palaeomagnetism. Amsterdam, Elsevier, 254-286.

Manuscript received May 2021;
revision accepted June 2022;
published Online September 2022.